Effect of microstructure on the indentation creep behaviour of 2.25Cr-1Mo and its comparison with modified 9Cr-1Mo ferritic steel

A thesis submitted in partial fulfillment of the requirements for the degree of
Master of Technology
in
Metallurgical and Materials Engineering
By

Manila Mallik

209MM1240

Department of Metallurgical and Materials Engineering
National Institute of Technology
Rourkela-769008

Effect of microstructure on the indentation creep behaviour of 2.25Cr-1Mo and its comparison with modified 9Cr-1Mo ferritic steel

A thesis submitted in partial fulfillment of the requirements for the degree of
Master of Technology
in
Metallurgical and Materials Engineering

Under the Supervision of

Prof. B. B. Verma and Dr.B.B. Jha

Department of Metallurgical and Materials Engineering
National Institute of Technology
Rourkela-769008

National Institute of Technology
Rourkela

CERTIFICATE

This is to certify that the thesis entitled, "***Effect of microstructure on the indentation creep behaviour of 2.25Cr-1Mo and its comparison with modified 9Cr-1Mo ferritic steel*** " submitted by Mrs. Manila Mallik in partial fulfillment of the requirements for the award of Master of Technology Degree in Metallurgical and Materials Engineering at the National Institute of Technology, Rourkela (Deemed University) is an authentic work carried out by her under my supervision and guidance. To the best of my knowledge, the matter embodied in the thesis has not been submitted to any other University/Institute for the award of any Degree or Diploma.

.

Prof. B.B. Verma

Dept. of Metallurgical and Materials Engg.

National Institute of Technology

Rourkela-769008

Dr. B.B. Jha

Scientist G, Surface Engg. Dept.

Institute of Minerals &Materials Technology

Bhubaneswar - 751013

Date: 06- 06- 2011

Acknowledgement

I avail this opportunity to express my heartfelt gratitude and regards to **Prof. B.B.Verma**, Department of Metallurgical & Materials Engineering, National Institute of Technology, Rourkela for his invaluable guidance, untiring efforts and meticulous attention at all stages during my project work. An erudite professor and a strict disciplinarian, I consider myself fortunate to have worked under his supervision.

I would also like to convey my deep regards to my co-supervisor **Prof. B.B. Jha, IMMT Bhubaneswar**, for his indebted help and valuable suggestions for the accomplishment of my dissertation work.

I am also grateful to **Prof. B.C. Ray, Prof A. Mallik** and **Prof. P. K. Ray** for his valuable suggestion to bring out this thesis in time.

My sincere regards to **Mr. T. Sahoo**, **Mr. R. Sahoo, Miss S. Parida, Mr. D. tripathy, Mr. M. Mukherjee IMMT Bhubaneswar**, for their co-operation during the period of work.

I am also thankful to **Mr. S. Hembram , Mr. R. Patnaik** and **Mr. U.K. Sahoo** Metallurgical & Materials Engineering, Technical assistants, for their help during the execution of experiment.

Last but not the least special thanks to my husband **Mr. S. Behera**, family members, labmates and special thanks to **Mr. S. Kumar** for his kind support.

Manila Mallik

TABLE OF CONTENTS

LIST OF FIGURES

LIST OF TABLES

Abstract

2.25Cr-1Mo and modified 9Cr-1Mo are extensively used for super heater and reheater tube, header pipe in large-scale thermal and nuclear power plant. Some of the important factors to be considered for selection of such steels are resistance to creep deformation, resistance to environmental attack, corrosion resistance, oxidation resistance. Long term exposure at elevated temperature and pressure can result in microstructural changes. The effective strength, i.e. load bearing capacity of the tubes due to microstructural damages decreases. The failure occurs when it falls below a critical level determined by component geometry and loading. The objective of the investigation is to study the effect of microstructure on the indentation creep behaviour of 2.25Cr-1Mo and its comparison with modified 9Cr-1Mo.

Indentation creep tests for 2.25Cr-1Mo ferritic steel and modified 9Cr-1Mo steel were carried out at different temperature and different load by using Spranktronics indentation creep testing machine. The microstructural examinations and phase analysis were carried out with the help of an image analyser. The microstructural examinations and EDAX were taken by SEM. Hardness measurements were done using a Vickers hardness tester by applying 500g load with dwell time of 15 s. The plates of two alloy steels were first normalised at 950°C for 2hrs. Indentation creep tests for 2.25Cr-1Mo ferritic steel were carried out at different temperature (480^0C, 500^0C, 520^0C) and different load (10 Kg, 20Kg). The indentation creep test of modified 9Cr-1Mo ferritic steel was done at 520^0C with a load of 10kg.

The results highlight that creep of 2.25Cr-1Mo ferritic steel was load and temperature dependent, larger load and higher temperature resulted in a larger creep deformation. It was also found that higher load and higher temperature caused higher creep rate .Creep rate for all temperature and loads had a maximum value at the initial creep stage and it decreased dramatically after a period of holding time. The value of activation energy was found to be 95kJ/mol. From the microstructural analysis it was revealed out that with increase in temperature there is a decline in creep strength because there is a reduction in the amount of bainite with the progress of temperature. Modified 9Cr-1Mo steel shows best compressive behaviour than 2.25Cr-1Mo.Because it contains more amount of alloying element.

***Key words*:** 2.25Cr-1Mo ferritic steel, Modified 9Cr-1Mo ferritic steel, Indentation Creep.

CHAPTER 1

Introduction

Chapter 1

1. INTRODUCTION

1.1. Background

2.25Cr-1Mo steel (SA2123-T22) and modified 9Cr-1Mo steel (SA335-P91) are also known as creep resistant steels because they do not sag even at high temperatures (550^0C-580^0C) [1]. These steel are key to the construction of steam generator components of liquid metal cooled fast breeder reactors and fossil fired power plants, chemical and petrochemical plants a long time [2]. These steel are used for elevated temperature header and piping as well as super heater and re-heater tubes in various power generating units (Fig.1.1). The selection of these structural material at elevated temperature is primarily based on a good combination of mechanical properties, high oxidation resistance, high creep resistance, high weld ability, high corrosion resistance, high thermal conductivity, low thermal expansion of coefficient and good resistance to stress corrosion cracking in steam and sodium environment systems compared to other steels [3-4].

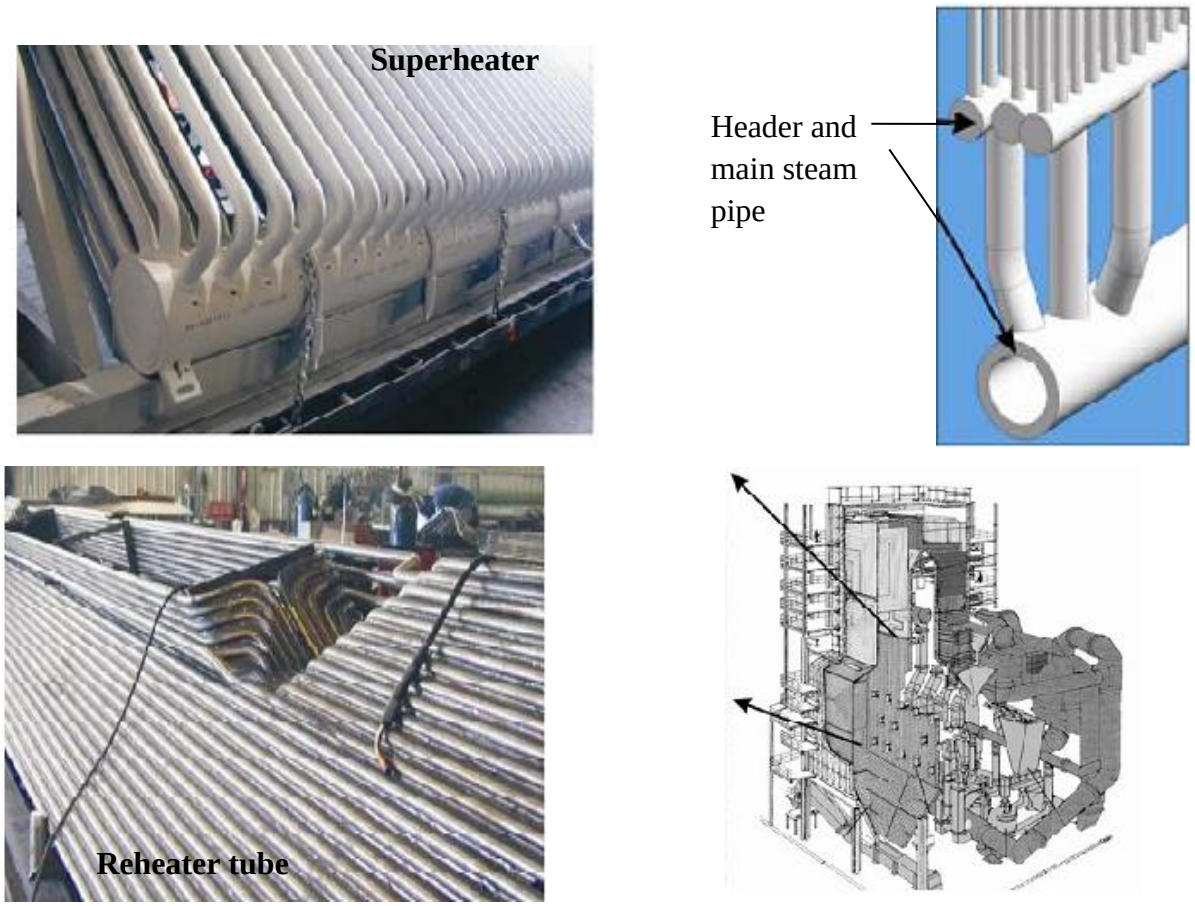

Fig.1.1 Schematic photographs of a fossil fired boiler and their

During the last decade , great progress has been made in developing creep-resistant steels of high strength and corrosion resistance at ever increasing temperature [5] . Although in the past, the driving force for the developments has been primarily to achieve higher efficiencies, the focus has been shifted more recently to the reduction of emission of CO_2, dioxins, and other environmental hazardous gases [6-9] by increasing the pressure and temperature.

The development of creep-resistant steels is a result of continous technological progress throughout the 20^{th} century [10]. The urgent need to improve creep strength of steels was based on endeavours by the power station industry to improve the thermal efficiency of steam power plant by raising the steam temperature and steam pressure in order to reduced the cost of fuel and reduce use of resources [11-16]. Since roughly 1900, the heat rate of thermal power plants in Germany has been reduced step-by-step increase in the steam parameters from 275^0C/12 bars to 620^0C/300 bars (Figure1.2).

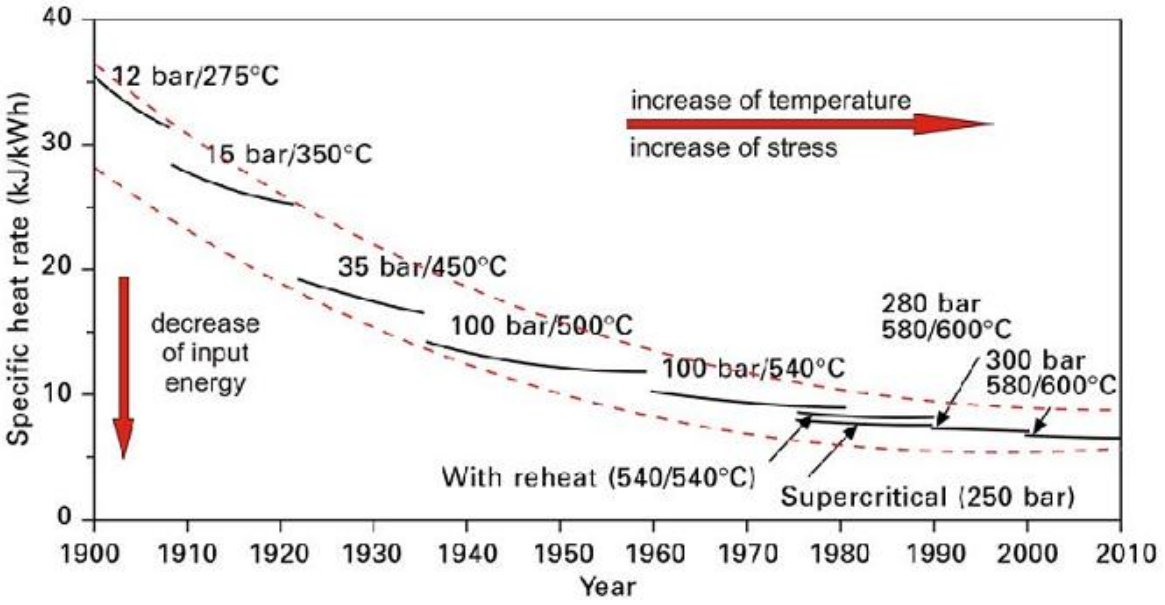

Fig.1.2 Heat rate of power steam plants in Germany as a function of steam parameters.

The thermal effect of fossil-fired power plant can be raised by reducing exhaust heat and heat transfer losses. The limit has virtually been reached for reducing exhaust heat losses, which are mainly through the condensers from cooling turbine and boiler exhaust [12]. Heat transfer losses, however, can be reduced by raising the pressure and temperature of the steam, but the extent to which can be done is greatly influenced by the materials Because of prolonged exposure to high temperatures, stresses and aggressive environments in power plants,

structural component have finite life. For these steel which are exposed to high temperature in power plants, creep strength in particular is of utmost importance. Creep is one of the important process occurring during prolong operation and it is responsible for accumulating microstructural damages in the tubes. The effective strength, i.e. load bearing capacity of the tubes due to microstructural damages decreases [14]. When the accumulation of damage exceeds a critical level, catastrophic failure will occur. The failure may lead to human loss, human injury and plant shutdown, which in turn will incurr economical loss. So my investigation is to study the effect of microstructure on indentation creep behaviour in 2.25Cr-1Mo and its comparison with modified 9Cr-1Mo ferritic steel and it will be a means to ensure avoidance of such failures. Several study has been carried out on oxidation [17], corrosion [18], fatigue [19], wear [20],**.** But the study on indentation creep test of these steel is relatively scanty compared to the vast data available on the creep behavior of these alloy . Although literature is available on creep behaviour in these steel, yet this will give some value-addition to the literature.

1.2. Objective of the project work

- ✓ To study the microstructure and tensile properties of normalised P91and T22 steel.
- ✓ To study the indentation creep behaviour in 2.25Cr-1Mo ferritic stee at different load (480^0C, 500^0C, 520^0C) and indentation creep behaviour in 2.25Cr-1Mo ferritic steel at different load (10kg,20kg) for
- ✓ To evaluate activation energy for indentation creep.
- ✓ Comparision of indentation creep behaviour between P91 and T22 steel at 520^0c with a load of 20kg.
- ✓ To study the amount of phases and hardness in pre and post indented creep specimens.

1.3 Flow chart of the Project work

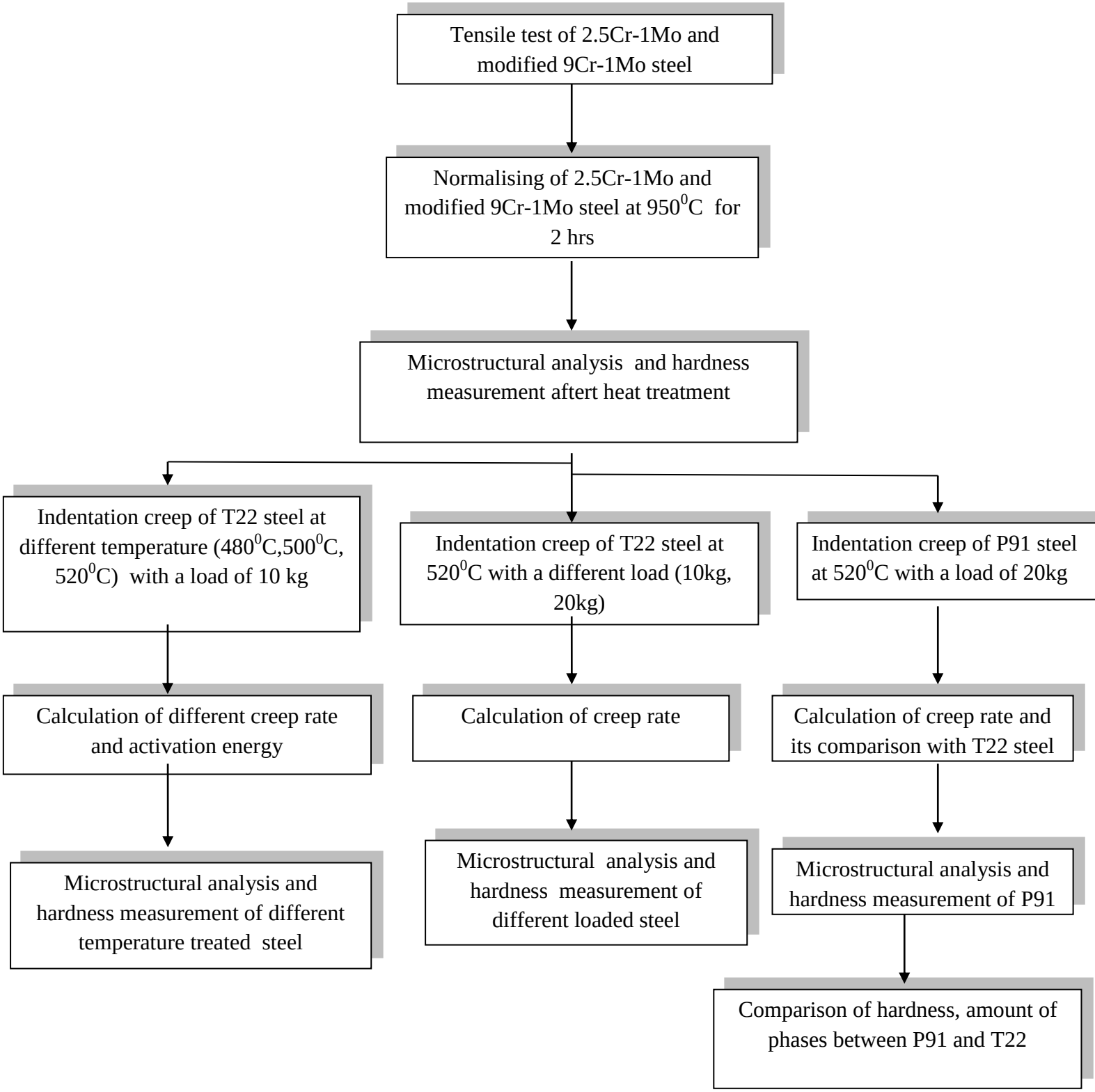

CHAPTER 2

Literature Survey

Chapter 2

2. LITERATURE REVIEW

2.1 Creep

Creep is defined as the progressive deformation at a constant stress [21]. It occurs below the yield strength of the material when it is exposed for long time to a high level of stress (Fig.2.1.). Creep is also more severe to those materials which are subjected to heat for long periods, close to melting point. Creep perpetually increases with increase in temperature. The rate of this deformation is a function of the material properties, exposure time, exposure temperature and also the applied structural load. Depending on the magnitude of the applied stress and its duration, the deformation might become so large that a component can no longer perform its function - for example creep of a turbine blade will cause the blade to contact the casing, resulting in the failure of the blade. Creep is sometimes of concern to engineers and metallurgists when determining components that are operating under high stresses or high temperatures. Creep is a deformation mechanism that may or may not constitute a failure mode. Sometimes moderate creep in concrete is welcomed as a result of it relieves tensile stresses which may otherwise lead to cracking. In contrast to brittle fracture, creep failure doesn't occur suddenly upon the application of stress. Instead, strain accumulates as a result of long-term stress .

Creep can be defined as time-dependent deformation at absolute temperatures greater than one half the absolute melting. This relative temperature (T (abs)/Tmp (abs)) is known as the homologous temperature. Several examples illustrate this point.

a) Ice melts at 0°C=273 K and undergo creep at -50°C=223 K. The homologous temperature is 223/ 273=0.82 which is greater than 0.5 so this is justified with the definition of creep.

b) Lead/tin solder melts at ~200°C=473 K and solder joints are known to undergo creep at room temperature of 20°C=293 K. The homologous temperature is 293/473=0.62 which is greater than 0.5 so this is also consistent with the definition of creep.

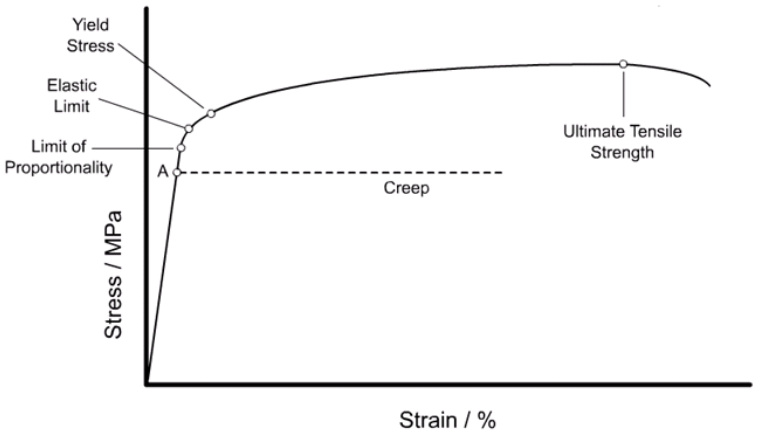

Fig. 2.1 Stress –strain diagram showing creep below the yield strength of the material due to long exposure to high levels of stress.

2.2 Creep curve

Relationship between strain and time at constant temperature is creep curve. (Fig.2) $\dot{\varepsilon} = d\varepsilon/dt$ = creep rate. ε_0= initial rapid elongation. Creep increases with time (primary creep) and reaches steady state (secondary creep) and finally increases rapidly with time until fracture occurs (tertiary creep).

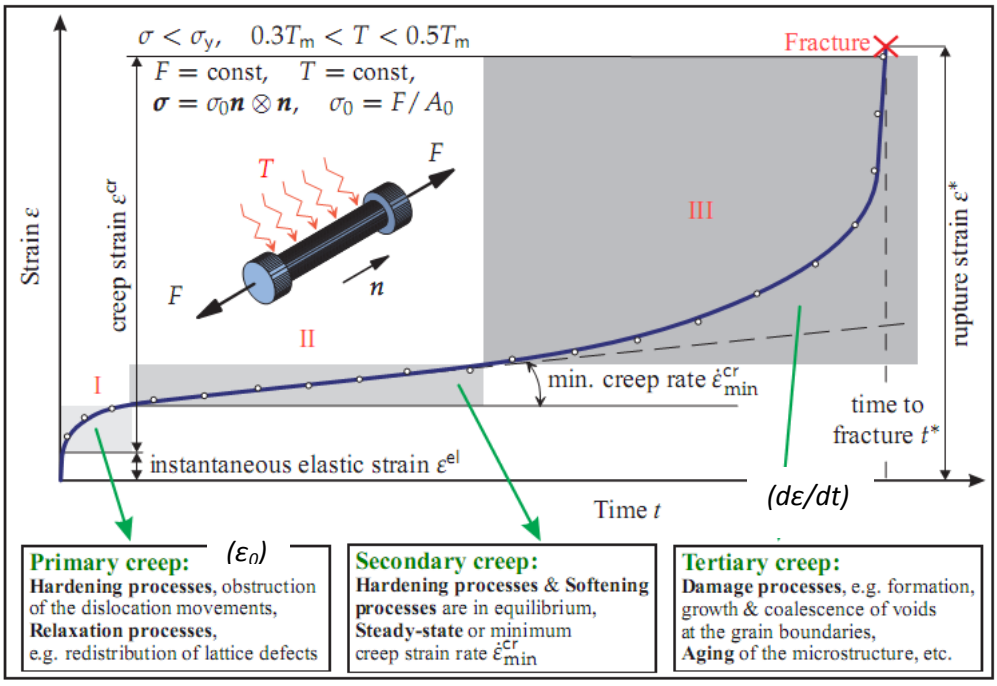

Fig. 2.2 Strain vs. time curve under constant load F and temperature T (I – primary creep, II – secondary creep, III – tertiary creep), after [22].

2.2.1Stages of creep

2.2.1.1 Primary creep

• It represents region of decreasing creep rate,

• It is period of transient creep.

2.2.1.2. Secondary creep

•It is period of nearly constant creep rate (steady state creep) which results from balance between strain hardening and recovery,

• It shows minimum creep rate.

2.2.1.3. Tertiary creep

• It occurs at high stresses at high temperature,

•It is associated with coarsening of precipitate particles, recrystallization, or diffusion,

• It shows high creep rate.

2.3 Models for Creep Curves

Table 2.1 Classical representations of primary, secondary and tertiary creep

Model equation	Source references
Primary creep	
Power law: $\varepsilon_f = At^p \longrightarrow \varepsilon_f = A\sigma^n t^p$	**Graham [23]**
Logarithimic: $\varepsilon_f = Blog(1+bt)$	**Philips [24]**
Exponential: $=C(1-exp(-ct))$	**Mc Vetty [25]**
Sinh law: $\varepsilon_f = Dsinh(ct^{1/3})$	**Conway [26]**
Secondary creep	
Power law : $\dot{\varepsilon}_{f,min} = A'\sigma^n$	**Norton [27]**
Sinh law: $\dot{\varepsilon}_{f,min} = \dot{\varepsilon}_0 sinh(\sigma/\sigma_0)$	**Nadai [28]**
Tertiary creep	
Eponential: $\varepsilon_f = M(exp(-mt)-1)$ $\dot{\varepsilon}_f = a\sigma^n/(1-\omega)^q$, *where* $\dot{\omega}=c\sigma^k/(1-\omega)^r$	**McHenry [29]** **Rabotnov-Kachanov [30,31]**
Omega: $\dot{\varepsilon}_f = \dot{\varepsilon}_0 exp(\Omega\varepsilon)$	**Sandstrom-Kondyr [32]**

A wide range of model for creep equations are in use today to represent the high-temperature time-dependent deformation behaviour of engineering materials. Many of these comprise components originating from a small number of classical representations of primary, secondary, and/or tertiary creep deformation [23-32], which has been shown in above Table 2.1.

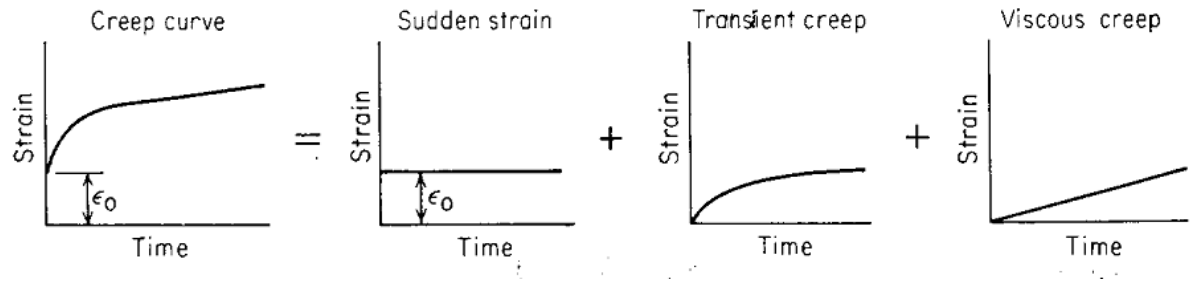

Fig.2.3 Andrade's analysis of the competing processes which determine the creep curve [21].

There have been several models proposed for creep curves. Andrade (1914) considered the superposition of a transient term (primary creep) and a viscous creep term (secondary creep), thus

$$\varepsilon = \varepsilon_i (1+\beta t^{1/3}) exp\ (kt) \quad \text{..... (1)}$$

where β is a constant for transient creep (primary creep) and k is related to the constant strain rate. A "better" fit is obtained by:

$$\varepsilon = \varepsilon_i + \varepsilon_t\ (1-exp\ (-rt)) + t\dot{\varepsilon}_{ss} \quad \text{.....(2)}$$

where r is a constant, ε_t is the strain at the transition from primary (transient) to secondary (viscous) creep and $\dot{\varepsilon}_{ss}$ is the steady-state strain rate. Although no generally-accepted forms of nonlinear strain-time relations have been developed, one such relation is:

$$\varepsilon = \varepsilon_i + B\sigma mt + D\sigma\alpha(1-exp(\beta t)) \quad \text{.....(3)}$$

where B, m, D, a and b are empirical constants.

In this relation, if $t > t_{transient}$ then

$$\varepsilon = \varepsilon_i + B\sigma mt + D\sigma\alpha \quad \text{.....(4)}$$

and the strain rate is the steady-state or minimum strain rate:

$$d\varepsilon/dt = B\sigma m = \dot{\varepsilon}_{ss} \quad \text{..... (5)}$$

The steady state or minimum creep rate is often used as a design tool. For example, what is the stress needed to produce a minimum creep rate of 10-6 m/m / h (or 10-2 m/m in 10,000 h) or what is the stress needed to produce a minimum creep rate of 10- 7 m/m / h (or 10-2 m/m in 100,000 h).

2.4 Structural changes during creep

Principal deformation processes during creep are slip, subgrain formation, and grain boundary sliding.

(1) Deformation by slip

(2) Subgrain formation

(3) Grain boundary sliding

(1) Deformation by slip: Slip under high temperature creep conditions occurs on many slip planes by operation of dislocation sources. Dislocations are line defects that slip through a crystal lattice when a minimum shear stress is applied. Dislocations initially slip along the closest packed planes in the closest packed directions since this requires the least energy or applied stress. An edge dislocation consists of an unfinished atomic plane, the edge of the plane being the line of the dislocation, and it is characterised by a Burgers vector, or 'misfit strain' at 90^{o} to the dislocation line. Screw dislocations have a Burgers vector parallel to the dislocation line and can slip on any close packed plane containing both line and Burgers vector, whereas edge dislocations only slip on the plane defined by the line and the perpendicular Burgers vector. Figure 2.4. shows formation of a slip step in the crystal due to slip of an edge dislocation.

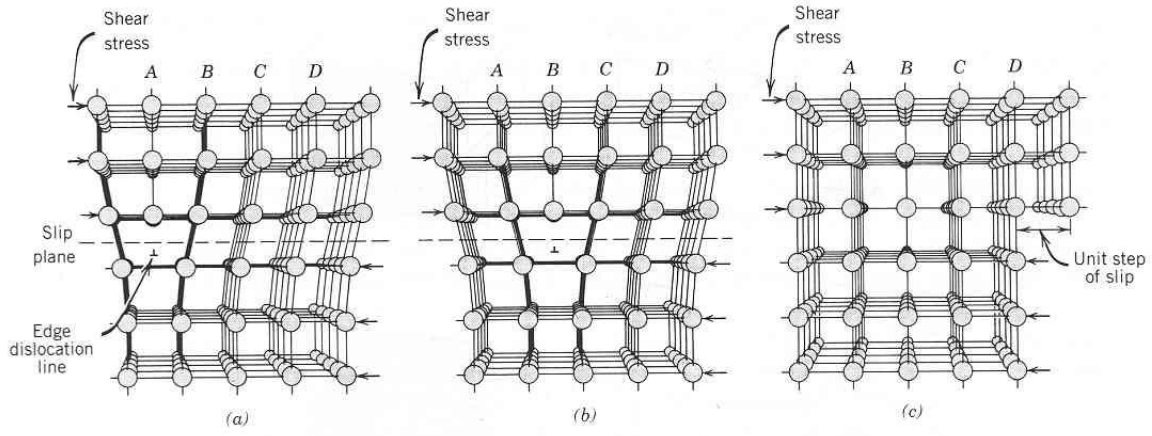

Fig.2.4 Showing formation of a slip step of an edge dislocation due to the application of shear stress.

When a polycrystalline metal is deformed then the grain that have slip planes suitably aligned to the applied stress, they undergo slip. It will occur in that grain when the shear stress exceeds the critical resolved shear stress. Dislocations multiply at sources, e.g. Frank-Read sources, and because the dislocation density increases, dislocation interact with each other.

Due to interaction dislocations may entangle or cut through one another, leaving slip steps on the dislocation lines referred to jogs, and if one amongst the dislocations is sessile, or immobile, the jogs will hinder slip. Dislocations arriving at grain boundaries might not be able to slip into the successive grain because of a unique orientation, and consequently form a 'pile-up' at the boundary. Any following dislocation are going to be repelled by the pile-up owing to the long-range elastic forces between dislocations of a same sign. The elastic strain energy per unit length of a dislocation is given by:

$$E = 0.5Gb^2 \quad \text{.....(6)}$$

where G is the shear modulus of elasticity and b is the Burgers vector.

(Compare this with macroscopic strain energy:

$$U = 0.5\sigma\varepsilon = 0.5E\varepsilon^2 \quad \text{..... (7)}$$

where E is Young's modulus).

If two dislocations of the same sign were to be moved together, their associated strain would double to $2b$, and the energy would quadruple to become

$$E = 0.5G(2b^2) = 2Gb^2 \quad \text{.....(8)}$$

hence the repulsion between dislocations which must be overcome by the applied stress. This and the above mechanisms contributes to work hardening of the metal, i.e. as the metal is deformed, plastic flow becomes increasingly more difficult and more stress has to be applied to accomplish it. In the primary stage of a creep test, the stress is constant and these mechanisms lead to a decreasing strain rate.

During secondary or steady state creep, the increased strain energy stored in the metal due to deformation, together with the high temperature, provides a driving force for the process of recovery. There is therefore a balance between the processes of work hardening and recovery. Recovery involves the reduction in dislocation density and the rearrangement of dislocations into lower energy arrays or sub-grain boundaries. In order for this to happen, dislocations have to climb as well as slip, and this in turn requires atomic movement or self-diffusion within the lattice. Self-diffusion is only possible in a close packed lattice if the atoms have enough energy to jump into a neighbouring site and if there is a vacancy at that site. As temperature increases atoms have more thermal energy (proportional to RT) and the equilibrium concentration of vacancies in a metal increases exponentially. The number of vacancies n_v , is given by:

$$n_v = n_0 \exp(-Qv/RT) \quad \text{.....(9)}$$

where n_0 is the number of lattice sites and Qv is the activation energy for vacancy creation and movement, (or the activation energy for self-diffusion). The rate of steady state creep

increases exponentially with increasing temperature, since its rate is controlled by vacancies, the numbers of which also increase exponentially with temperature. Figure 2.5 shows the mechanism of self-diffusion by vacancy movement.

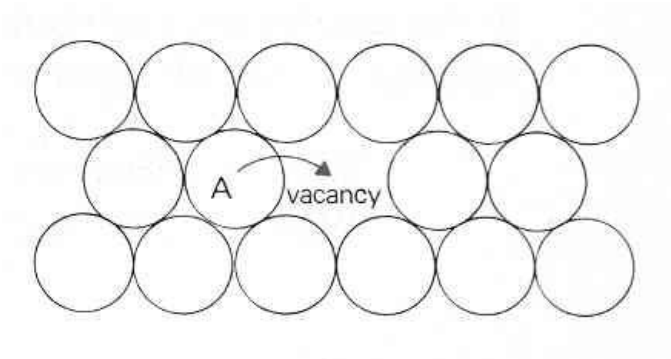

Fig.2.5 Vacancy movement or selfdiffusion.

Dislocations slip is hindered by obstacles such as (i) grain boundaries, (ii) impurity particles, (iii) the stress field around solute atoms in solution or (iv) the strain fields of other dislocations. Pile-ups may form at obstacles as shown in Figure. 2.6.

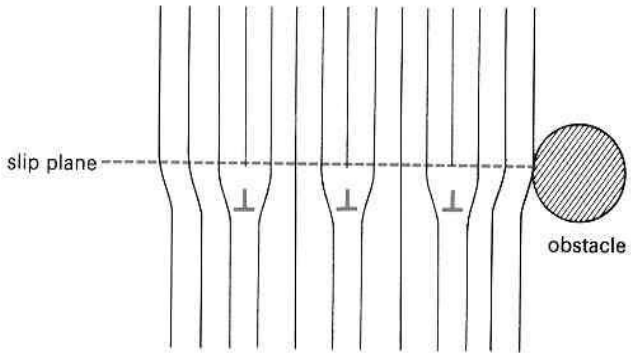

Fig.2.6 Pile-up of dislocations at an obstacle.

Vacancies diffusing onto the bottom of dislocations will cause jogs in the dislocation, but eventually when the whole line of atoms along the bottom of the dislocation extra plane have diffused away, the dislocation will have climbed normal to its slip plane by one atomic spacing. When the dislocation has climbed to an unobstructed slip plane, it will then be free to slip past the obstacle. Dislocations of opposite sign attract each other and by a process of climb and slip can move together and annihilate each other. Dislocations of the same sign, by similar processes, will align vertically above each other into a dislocation wall. This occurs because the stress field around an edge dislocation is compressive above the slip plane and tensile below, so aligning vertically tends to balance out these stress fields and reduces the

total energy of interaction. A dislocation wall is in effect a low angle tilt boundary and evidence from X-Ray diffraction, optical and electron microscopy shows that the grains in a metal become sub-divided into sub-grains (called polygonisation) during steady state creep. These processes are illustrated in Figures. 2.7 to 2.10.

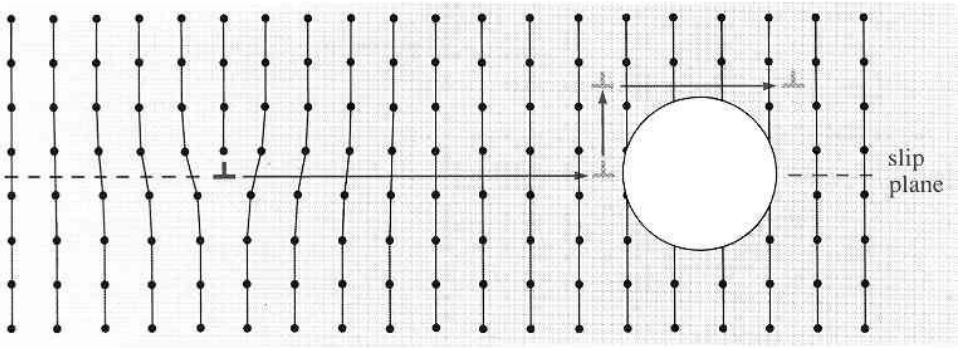

Fig.2.7 Dislocation climb and slip past an obstacle.

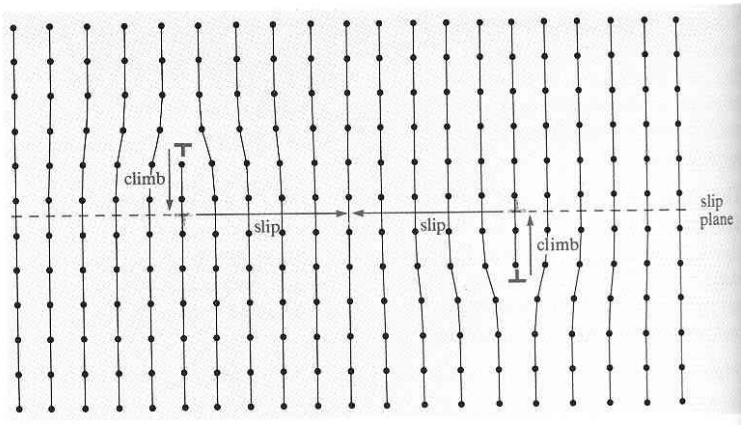

Fig.2.8 Dislocations of opposite sign climb and slip to annihilation.

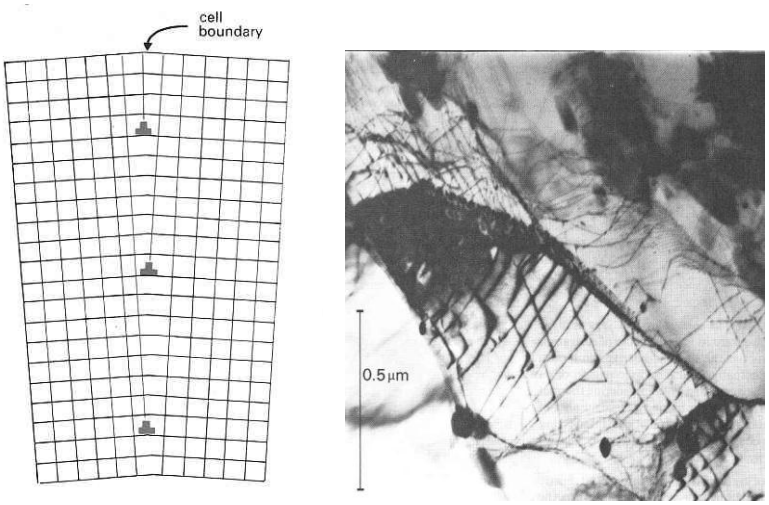

Fig2.9 (right) Dislocation wall produced during recovery by slip and climb and Fig. 2.10

(left) Sub-grain structure in 12% chromium steel produced during steady state creep, revealed by transmission electron microscopy (TEM).

The above mechanisms represent only part of the picture. The situation in solid solutions is more complex due to the strain fields around solute atoms. Climb is, however, still the basic controlling mechanism in steady-state creep of solid solution alloys.

(2) Sub-grain formation: Dislocations arrange themselves into low angle grain boundary. Sub grain size depends on stress and temperature, that is, large sub grains are produced by high temperature and low stress or low creep.

(3) Grain boundary sliding: It is shear process which occurs in direction of grain boundary• occurs along grain boundary as movement of two grains. The onset of tertiary creep is a sign that structural damage has occurred in an alloy. Rounded and wedge shaped voids are seen mainly at the grain boundaries (Figure. 2.11.), and when these coalesce creep rupture occurs. The mechanism of void formation involves grain boundary sliding which occurs under the action of shear stresses acting on the boundaries. (Figures.2.12, 2.13 and 2.14).

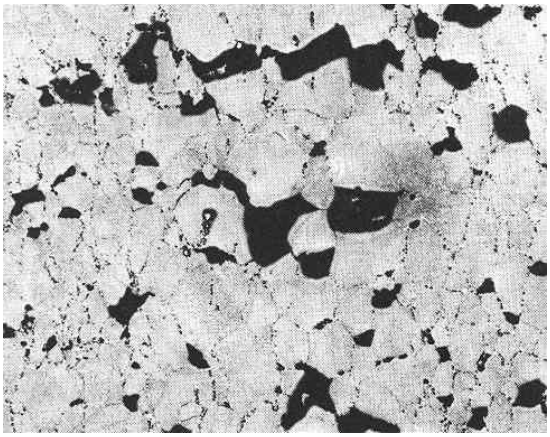

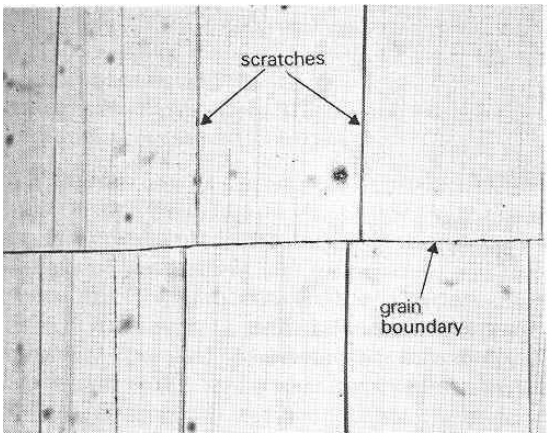

Fig.2.11 (left) Voids in creep ruptured Nimonic 80A. (1023 K and 154 MNm-2) X150.
Fig.2.12 (right) Showing scratch lines displaced across a grain boundary in aluminium.

Evidence for grain boundary sliding is the displacement of scratch lines during creep testing (Fig.2.12).

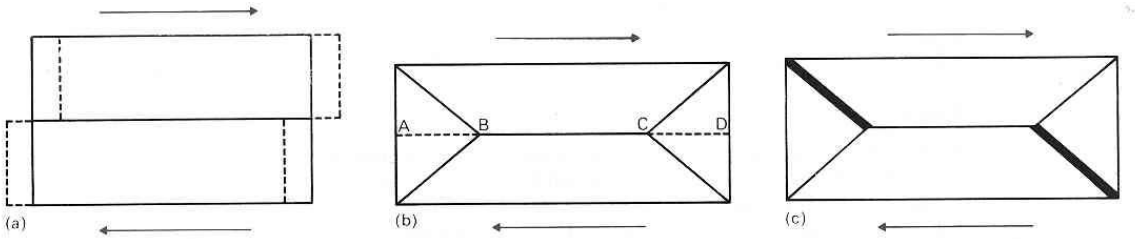

Fig.2.13 A model for the formation of cracks due to grain boundary sliding.

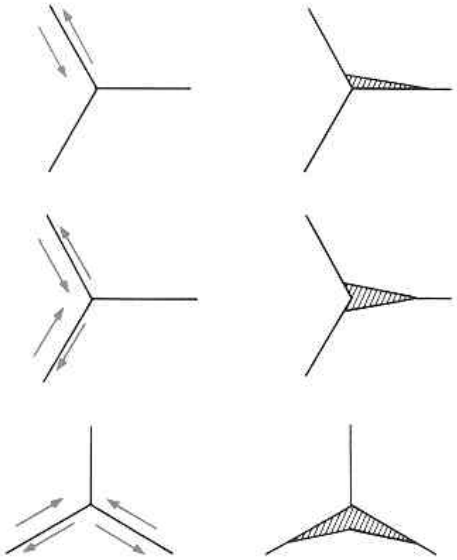

Fig.2.14 The formation of wedge cracks during grain boundary sliding.

The more rounded voids are possibly produced where there is a step on the grain boundary which initially gives a square void as the grains slide, but this is rounded off by diffusion which reduces the surface area and energy of the void. The grain boundary sliding may account for 10% to 65% of the total creep strain, the contribution increasing with increasing temperature and stress and reducing grain size. Above about 0.6 Tm the grain boundary region is thought to have lower shear strength than the grains themselves, probably due to the looser atomic packing at grain boundaries. Boundaries lying at about 45^{o} to the applied tensile stress experience the largest shear stress and will slide the most. Vacancy or atomic diffusion along the boundary is also easier, and may play a role in sliding since it has been observed that processes such as ordering and precipitation which makes slip within the grains more difficult, also decrease the grain boundary strain contribution by the same factor.

2.5 Mechanisms of creep

(1) Diffusion creep- At low stresses, $\sigma/G < 5\text{x}10^{-6}$, linear dependence on stress (n=1) is obseved.→ Harper-Dom creep.

(2) Dislocation creep- At medium stress, $5x10^{-6}<\sigma/G < 10^{-3}\rightarrow$ power law creep (n=5)

(3) Dislocation glide- At high stresses, $\sigma/G > 10^{-3}$, power lawbreaks down → Sellars-Tegart creep, $\acute{\varepsilon}_s = AD/(\alpha^n b^2)$ (sinh ασ/E)n.....(10)

where $\alpha = (\sigma/E)^{-1}$

(4) Grain boundary sliding involves the sliding of grain past each other.

(1) Dislocation glide- Dislocations move along slip planes and overcome barriers by thermal activation at high stress ($\sigma/G > 10^{-2}$). Dislocations are impeded by obstacles such as precipitates, solute atoms, and other dislocations.

(2) Dislocation creep- Dislocations overcome barriers by thermally assisted mechanisms involving diffusion of vacancies or interstitials at $10^{-4}< \sigma/G < 10^{-2}$.Steady state creep rate was suggested by Orowan and Bailey,$\acute{\varepsilon}_s$= (strain hardening rate, $h = d\sigma/d\varepsilon$)/(thermal recovery rate, Gittus proposed a mechanism based on diffusion aided movement of dislocations

$$\acute{\varepsilon}_s = 16\pi^3 c_j DvGb/(kT)\ (\sigma/G)^3 = ADvGb/(kT)\ (\sigma/G)^n \text{.....(11)}$$

power law relation ,where c_j= concentration of jogs, Dv= bulk or lattice self-diffusion coefficient, G = shear modulus. The diffusion coefficient Dv can be described by

$$Dv = D_0 exp(-Q/kT)$$

(3) Diffusion creep - occurs by transport of material by diffusion of atoms within a grain. Like all diffusional processes, it is driven by a gradient of free energy (chemical potential), created in this case by the application of stress.

There are two types of diffusion creep, depending on whether the diffusion paths are predominantly through the grain boundaries, termed *Coble creep* (favoured at lower temperatures) or through the grains themselves, termed *Nabarro-Herring creep* (favoured at higher temperatures).

Coble creep is a form of diffusion creep, it is the mechanism for deformation of crystalline solids. Coble creep is due to the diffusion of atoms in a material along the grain boundaries, which produces a net flow of material and a sliding of the grain boundaries. The strain rate in a material experiencing Coble creep is given by:

$$\dot{\varepsilon}_s = 50\sigma b^4 Dgb/kTd^3 \quad \text{.....(12)}$$

Where

d is the grain diameter and *Dgb* is the grain boundary diffusion coefficient [21].

Nabarro-Herring creep is one of the forms of diffusion controlled creep. In Nabarro-Herring creep, diffusion of atoms through the lattice resulting grains to elongate along the stress axis; *k* is stated to the diffusion coefficient of atoms through the lattice, *Q = Q(self diffusion), m* = 1, and *b* = 2. Therefore Nabarro-Herring creep includes a low stress dependence and a moderate grain size dependence, with the creep rate decreasing as grain size is increased. Nabarro-Herring creep is strongly temperature dependent. For lattice diffusion of atoms in a material, should additionally overcome the energy barrier and for this movement the neighboring lattice sites or interstitial sites in the crystal structure must be free. For the movement of atom , it must also overcome the energy barrier to move its current site (it lies in an energetically favourable potential well) to the nearby vacant site (another potential well). The generalised form of the diffusion equation is

$$D = D_0 exp(-E/kT) \quad \text{.....(13)}$$

where D_0 is dependent upon the jump frequency and also the number of nearest vacant sites. Therefore D_0 is a double dependence upon temperature. At higher temperatures , there is a increment in vacancies through Scottky defect formation so as a result of this diffusivity increases and an increase in the average energy of atoms in the material. Nabarro-Herring creep is observed at very high temperatures as compared to a material's melting temperature.

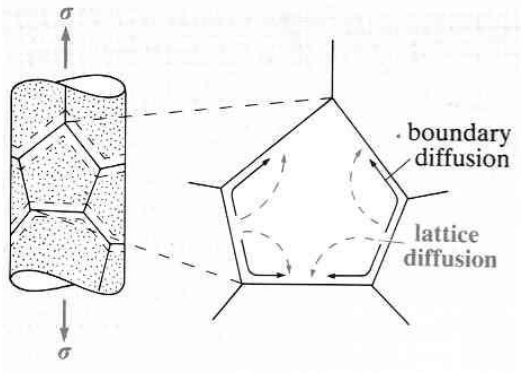

Fig. 2.15 Diffusional flow .

(4) Grain boundary sliding

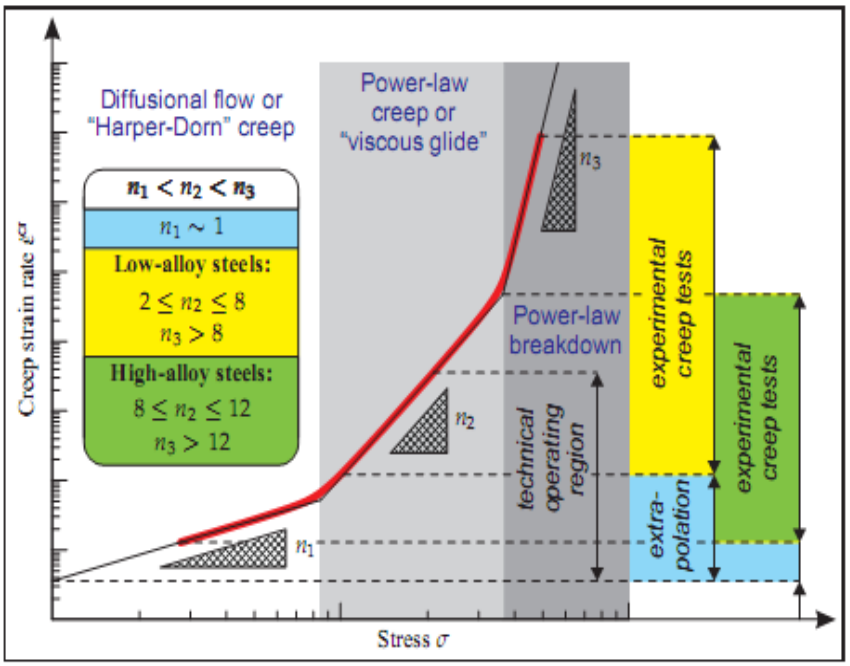

Fig.2.16 shows steady state creep rate depending on stress.

While Grain boundary sliding does not contribute significantly to steady-state creep,it is important in initiating inter granular fracture (Fig.2.17).

2.6 Indentation creep

The indentation creep test provides a simple and non-destructive method of investigating the mechanical proper-ties of solids, it also gives information about the time dependent flow of materials [33-36]. In this test, the indenter is maintained at a constant load over a period of time under well-controlled conditions. As the stresses cause the material beneath the indenter to creep, the indenter penetrates and changes in the indentation size are monitored. Thus, indentation creep is the time dependent motion of a hard indenter into a solid under constant load [37,38].

2.6.1 Advantage of the indentation creep

1. The indentation creep technique is that all the creep information can be collected from the same sample, which not only greatly reduces the effort for sample preparation but also reduces the sample to sample variation in property [39].

2. This technique can be used for studying the creep properties of high temperature materials such as intermetallics and ceramics, including diamond, which are very difficult to evaluate using conventional methods.

3. Indentation method can be regarded as a quick and non-destructive procedure to extract information on the mechanical behaviour of materials

The indentation test performed with hemishperical indenter for the measurements of viscosity of glasses was applied by Heynes and Rawson in the 60s [38]. The theoretical interpretation of this measurement was worked out by Douglas a few years later [39]. Nevertheless, in spite of its obvious advantages, the method hasn't got widely applied because of difficulties of the measurement techniques at that time.

The indentation creep test performed with flat ended cylindrical punch was originally proposed by Yu and Li in the 70s for investigation of creep properties of materials. Using this method for the investigation of high temperature plasticity of single crystals they have proved that its results are equivalent to those of the tensile creep test [40,41]. During this measurement a cylinder is pressed to the flat surface of the sample (Fig. 2.17) and the depth of the indentation is registered as the function of elapsed time.

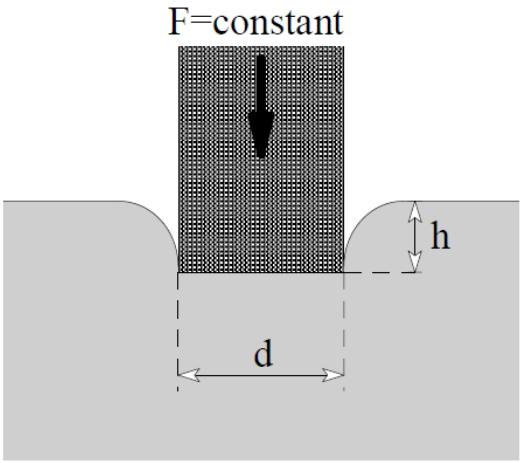

Fig. 2.17 Scheme of the indentation creep with cylindrical punch.

Fig. 2.18 shows a schematic creep curve taken during an indentation test performed by a flat ended cylindrical punch. Applying constant load, *F*, at constant temperature, *T*, after a short initial transient the punch penetrates at a constant impression velocity, *v*, into the sample. In comparison with the tensile creep test (Fig. 2.19) this curve contains also the stages characterizing the primary and secondary creep, but the accelerating stage of tertiary creep is missing, the deformation is stable to the last. This similarity led several authors to the assumption of the correspondence between the indentation and tensile creep [40-45].

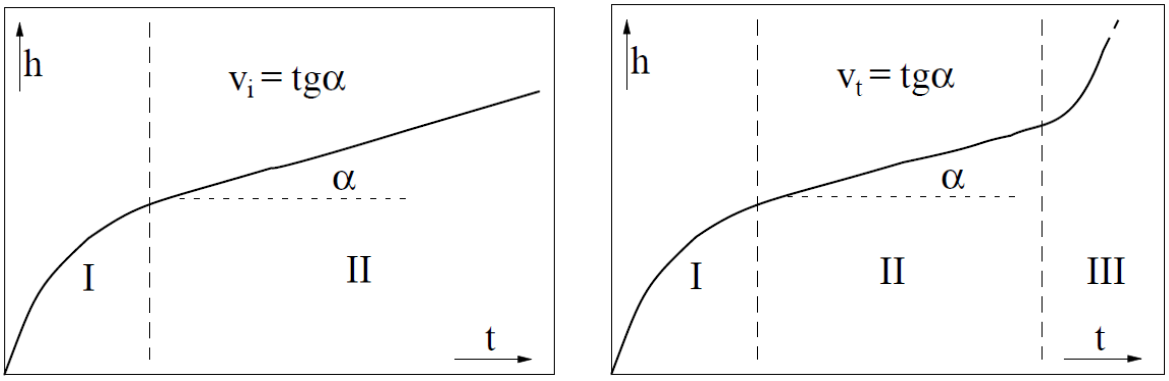

Fig 2.18 (right) Schematic indentation creep curve obtained by constant loading of a cylindrical punch and Fig. 2.19 (left) Schematic tensile creep curve.

Yu and Li investigated different types of materials as e.g. LiF and tin single crystals [40,41] and found correspondence between their tensile and indentation creep behavior. Using the idea of Yu and Li a relatively simple indentation creep equipment was constructed at the Department for General Physics of ELTE, by which superplastic SnPb and Al alloys were investigated [46-49] using only cylindrical indenters. The temperature interval of the applicability of this equipment was between room temperature and 650°C at an accuracy of ±5°C, therefore the range of the investigated materials was restricted to those, which have relatively low activation energy and high ductility at low temperature. Another essential disadvantage was the low accuracy of the indentation depth measurement.

2.6.2 Stress and strain distribution below the indenters

To establish an analytical relationship between the tensile and indentation creep requires experimental and theoretical investigation of the local stress and strain fields below the indenter is needed, which can provide physical basis of the correspondence. For the case of the cylindrical indenter a simple analytical description of the elastic stress field below the punch was given by Sneddon in the 60s [50]. Observations about existence and the propagation of plastic deformation zone have been reported for cast age-hardenable Al alloys [51] as it is shown in Fig.2.21. The stress and strain field below cylindrical indenters was studied by the finite element modelling (FEM) in the 90s [52] although the understanding and modelling of the appearance and forming of the local plastic and elastic deformation has not been investigated satisfactorily.

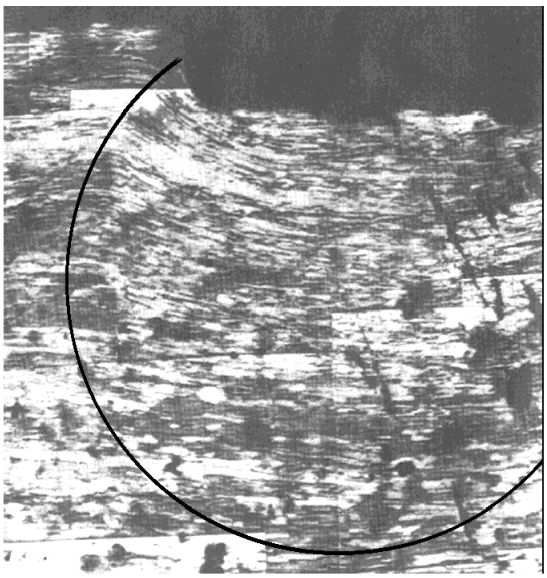

Fig. 2.20 Approximately spherical deformation zone in Al alloy.

It is worth noting that at relatively high local values of plastic strain the structural materials, e.g. composites may show different deformation behavior from the tensile ones, because during the tensile tests the rupture of the sample occurs at lover strain values.

2.6.3 Indentation creep tests on metals performed using cylindrical indenter[53]

High temperature mechanical behavior of metallic materials has also been investigated by indentation creep measurements. Indentation tests were performed with flat ended cylindrical punches on pure metals and on alloys. It is well known that high temperature creep of metallic materials can be described by the

$$\dot{\varepsilon} = A\sigma^n \quad \text{..... (14)}$$

power-law in a wide range of the strain rate. Eq. (14) describes the relationship between the strain rate, $\dot{\varepsilon}$, and the tensile stress, σ , at a constant temperature during the steady state creep (secondary creep). The n stress exponent and the A constant depend on the temperature, microstructural features and the activation energy of the deformation process.

In this study, the indentation creep behavior of Al-22U-2Zr and Al-46U-3Zr (composition in wt %) alloys was studied in the temperature range 693-783K at different stresses. These creep curves show a wavy pattern. The reason for this is that microstructure is not stable at the creep testing temperature. The stress component was found to be 5 [53].

2.6.4 Effect of stress and temperature

For isothermal tests, the shape of the curves for increasing stress may changes from dominant steady state to sigmoidal response with little steady state to dominant primary. Some of the similar trends are shown in Fig. 2.21.

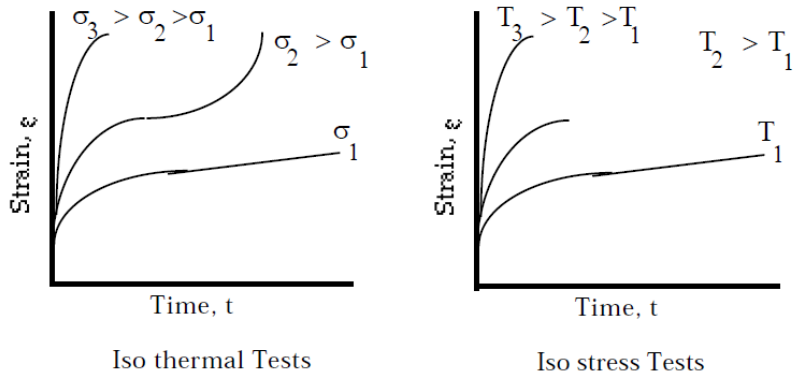

Fig.2.21 Effect of stress and temperature on strain time creep curves.

For isothermal tests,

$$\acute{\varepsilon}_{ss} = \acute{\varepsilon}_{min} = B\sigma^{n} \quad \text{..... (15)}$$

Above mentioned equation can be linearized by taking logarithms of both sides such that

$$Log\ \acute{\varepsilon}_{ss} = log\ \acute{\varepsilon}_{min} = log\ B + n \quad \text{..... (16)}$$

Log-log plots of $\acute{\varepsilon}_{ss} = \acute{\varepsilon}_{min}$ versus σ (fig.2.22.) often results in a bilinear relation in which the slope, n, at low stresses is equal to one indicating the mechanism is diffusion creep and n at higher stresses is greater than one indicating the mechanism is power law creep with mechanisms other than pure diffusion (e.g., grain boundary sliding).

For iso stress tests, the power dependence of stress becomes a constant resulting in

$$\acute{\varepsilon}_{ss} = \acute{\varepsilon}_{min} = C\ exp(-Q/RT) \quad \text{..... ....(17)}$$

this can be linearized by taking natural logarithms of both sides such that

$$\ln \acute{\varepsilon}_{ss} = ln\ \acute{\varepsilon}_{min} = ln\ C - Q/RT \quad \text{.....(18)}$$

Log-linear plots of $\acute{\varepsilon}_{ss} = \acute{\varepsilon}_{min}$ versus1/T (fig.2.23.) results in a linear relation in which the slope is equal to $-Q/R$ is related to the activation energy, Q, for creep.

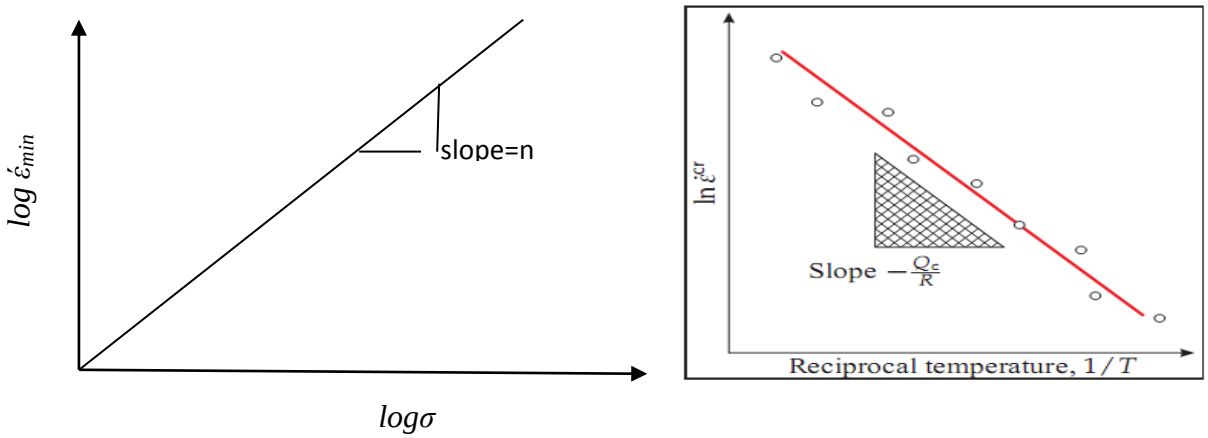

Fig.2.22 Log-log plot of $\acute{\varepsilon}_{ss} = \acute{\varepsilon}_{min}$ versus σ and Fig.2.23 Log-log plot of $\acute{\varepsilon}_{ss} = \acute{\varepsilon}_{min}$ versus1/T.

CHAPTER 3

Experimental & Procedure

Chapter 3

3. MATERIALS AND METHODS

3.1 Materials

2.25Cr-1Mo and modified 9Cr-1Mo steel were taken for the present investigation. They were prepared from 12mm plate of 2.25Cr-Mo and 16mm plate of modified 9Cr-1Mo low alloy ferritic steel respectively. Chemical compositions of these steels are given in Table 1. and Table 2.

Table: 3.1. Chemical composition of 2.25Cr-1Mo steel

Element	Cr	Mo	C	Mn	Si	S	P	Ni
wt %	2.25	0.98	0.07	0.42	0.019	0.025	0.02	0.02

Table: 3.2. Chemical composition of modified 9Cr-1Mo steel

Element	Cr	Mo	C	Mn	Si	P	S	Ni	V
wt %	9	0.99	0.09	0.35	0.25	0.02	0.01	0.4	0.19

3.2 Experimental Methods

A sample preparation for metallographic study is one of the key areas in materials research and development. The surface of a metallographic specimen is prepared by various methods sush as grinding, polishing, and etching. After preparation, it is often analyzed using optical or electron microscopy. Metallography deals with study of a materials microstructure. Analysis of a materials microstructure aids in determining if the material has been processed properly and is therefore a vital step for determining product reliability and for determining why a material failed. The essential steps for proper metallographic specimen preparation contains:

Sampling → rough grinding → intermediate polishing → fine polishing → etching → microstructural analysis

3.2.2 Scanning Electron Microscope (SEM)

The scanning electron microscope (SEM) has been a well accepted tool for many years in the examination of surfaces. The prominent imaging advantages are the great depth of field and high spatial resolution and the image is relatively easy to interpret visually.

Principle: A finely targated electron beam scanned across the surface of the sample generates secondary electrons, backscattered electrons, and characteristic X-rays. These signals are collected by detectors to create images of the sample displayed on a cathode ray tube screen. Options seen within the SEM image might then be immediately analyzed for elemental composition using EDS or WDS. The electrons that are emitted from the specimen surface have a spectrum of energies. Secondary and backscattered electrons are conventionally separated according to their energies. When the energy of the emitted electron is less than about 50eV, it is referred as a secondary electron and backscattered electrons are considered to be the electrons that exit the specimen with energy greater than 50eV. A critical point in understanding the formation of SEM images of fracture surfaces, and their interpretation, is an appreciation of the factors that affect this excited volume of electrons in the specimen [57]. To understand the different failure mechanisms in FRP composites, photomicrographs were taken using a SEM. There is a dramatic change in the structure and properties of the composite when exposed to high and low temperatures.

3.2.3. Indentation creep test

The indentation depth is measured by an LVDT (linear variable differential transformer) which is contacted mechanically to the weight holder plate . It can be used for measuring in a 1.5 mm displacement range with high linearity. The LVDT is directly connected to an 18 bit ADC (analog digital converter) data acquisition PC-card. The digital data served by the PC-card are processed and recorded to ASCII data files by a DOS-based measurement program. Further data processing can be performed by any other commonly used data analysis program e.g. Origin. The uncertainty of the displacement measurement is less than ±0.1 micron, the minimum sampling period is 0.4 sec. It can be seen that the resolution of the ADC is approximately 0.0125 micron and each point is are within the ± 0.1 micron interval.

3.3 Experimental Procedure

Sample orientation for tensile test, which details are given in Fig.3.1. Sample blanks with dimension (20 × 20 × 5) mm were cut by using power saw (Fig.3.2). Then the specimens were normalised in a carbolyte furnace by heating at a temperature of 950°C for a soaking period of 2hrs and cooled in air. The specimens were first ground using a belt grinder, then polished by emery papers (180, 280, 380, 400, 600, 1000, 1200, 1500) and finally polished using cloth polisher up to a surface finish of 25 μm. 2.25Cr-1Mo steel was then etched with freshly prepared nital's reagent (2% nitric acid in methyl alcohol) and modified 9Cr-1Mo steel was etched with freshly prepared Vilella's reagent (1gm picric acid, 5ml HCl, 100ml ethanol).

Gauge length= 50mm

W= 12.5mm

T= 12.5mm

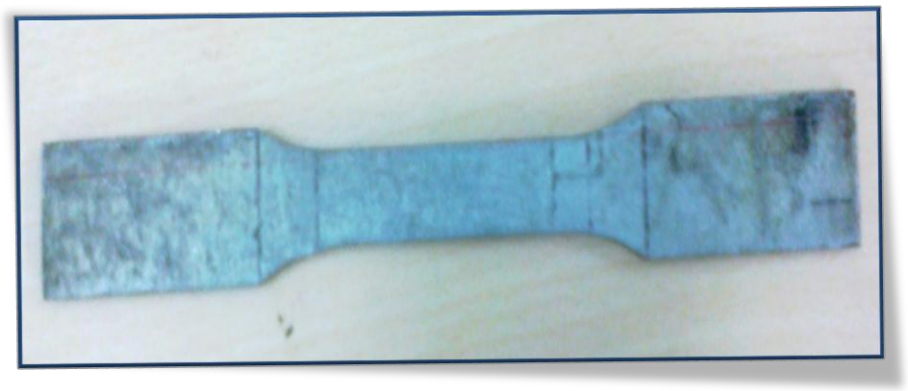

Fig. 3.1 Schematic diagram of Tensile Specimen.

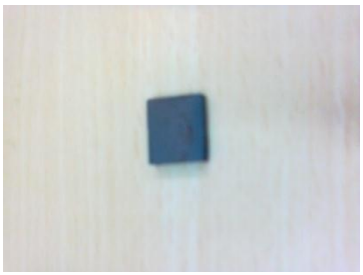

(20 × 20 × 5) mm

Fig. 3.2 Schematic diagram of Indentation creep specimen Specimen.

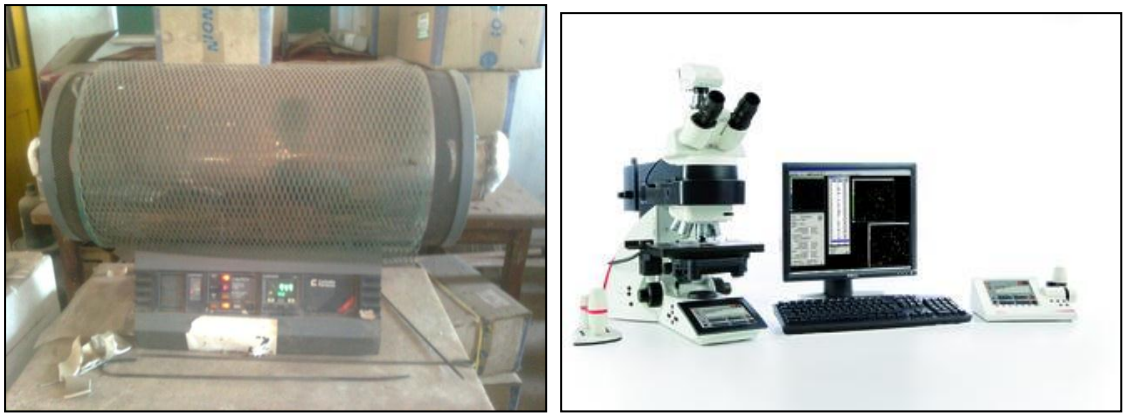

Fig. 3.3 The schematic picture carbolyte furnace and image analyser.

3.3.1. Tensile test analysis

Tensile test was carried out with the help of servo hydraulic INSTRON 8800 testing machine. Specimens were prepared according to ASTM E8M-04.

3.3.2. Microstructural Analysis

The microstructural examinations (microstrictural analysis, phase analysis) were carried out with the help of an image analyser (Model: Olympus DMI3000M).

3.3.3 SEM Analysis

The different micrographs of the tested samples were carried out using a JEOL-JSM 6510 LV SEM. The samples were loaded onto the sample holder and placed inside the SEM, adjusting the working distance and hence the spot size the chamber was closed and vacuum was applied.

3.3.4. Hardness Analysis

The hardness measurements were done with the help of a Vickers hardness tester (Leco MICROHARDNESS TESTER LM247AT) using an indentation load of 500g with a dwell time of 15sec.

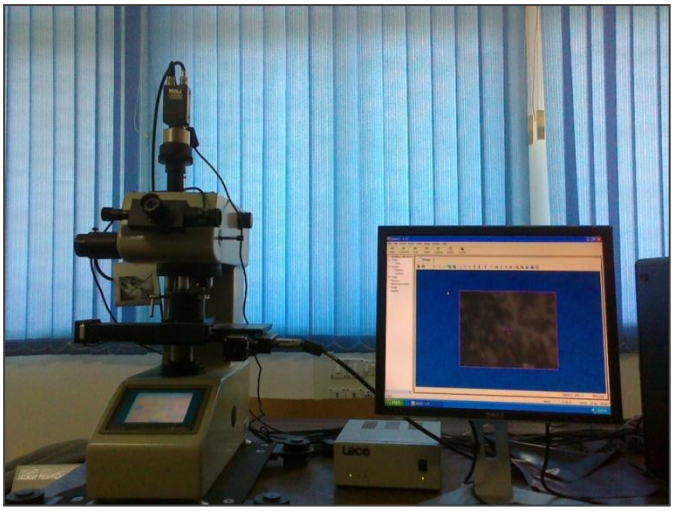

Fig. 3.4 The schematic picture of microhardness tester.

3.3.5. Indentation creep test Analysis

The indentation creep tests were carried out on a Spranktronics Indentation creep testing machine , which contains a constant-load equipment, a temperature controller and an experiment data collector. The cylindrical indenter dia. of 1.5mm is made from tungsten carbide, which is readily available and does not creep in the stress and temperature of the present study. The Indentation creep tests were performed under a variable load and variable temperature. The Indentation creep tests were performed under different load (ranging from10kg,20kg) and different temperature (ranging from 480^0C, 500^0C, 520^0C) for 2.25Cr-1Mo steel and the tested load and temperature was 20kg and 520^0c respectively for modified 9Cr-1Mo steel.

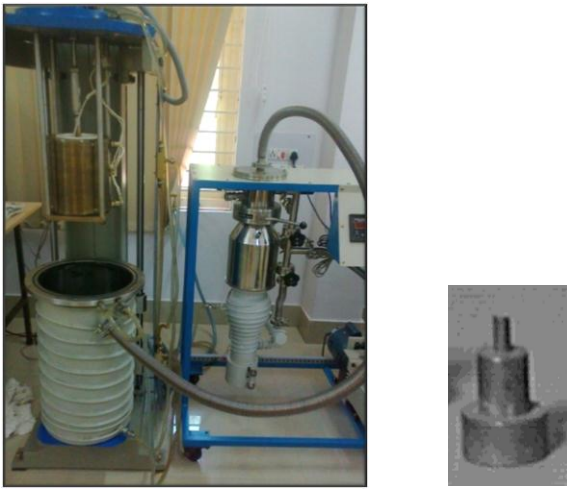

Fig. 3.5 The schematic picture of indentation creep tester and indenter.

CHAPTER 4

Results &Discussions

4. RESULTS AND DISCUSSION

The characteristics of microstructural feature, conventional mechanical properties of normalized 2.25Cr-1Mo and normalized modified 9Cr-1Mo ferritic steel is described in section 4.1. The creep behaviour, characteristics of microstructural feature, phase analysis, hardness of 2.25Cr-1Mo ferritic steel at different temperatures (480^0C, 500^0C, 520^0C) with a constant load of 10kg are described in section 4.2. The same analysis for 2.25Cr-1Mo ferritic steel at different load (10kg, 20kg) with a constant temperature 520^0C are described in section 4.3. While the creep behaviour , characteristics of microstructural feature ,phase analysis, hardness between 2.25Cr-1Mo and modified 9Cr-1Mo steels at 520^0C with a load of 20kg are described in section 4.4. The responses of above sections are described below.

4.1 Normalized 2.25Cr-1Mo and normalized modified 9Cr-1Mo ferritic steels

4.1.1 Microstructural Analysis

Typical optical and SEM micrographs of normalized 2.25Cr-1Mo and modified 9Cr-1Mo ferritic steels are illustrated in Fig. 4.1and Fig. 4.2 respectively. The white colour refers to ferrite and black colour refers to bainite and the reverse is true in SEM. The microstructure of the investigated normalized 2.25Cr-1Mo steel revealed that bainite is distributed in the ferrite matrix and the dispersion of bainite within ferrite matrix was finer in normalized modified 9Cr-1Mo ferritic steel. This is because normalized 9Cr-1Mo steel contains V and more amount of Cr than normalized 2.25Cr-1Mo steel.

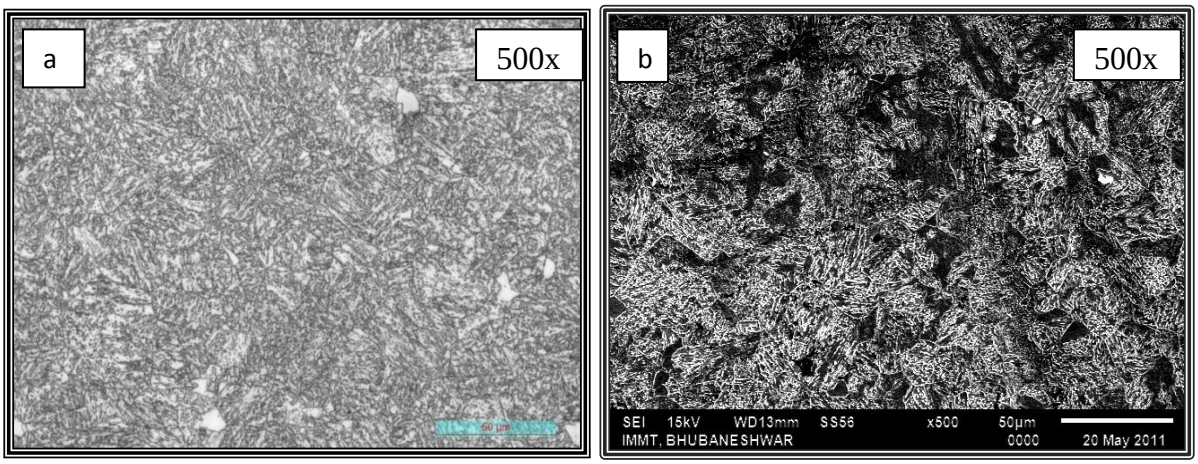

Fig.4.1 (a) Optical micrograph of normalized 2.25Cr-1Mo ferritic steel at 500X (b) SEM micrograph of normalized 2.25Cr-1Mo ferritic steel at 500X.

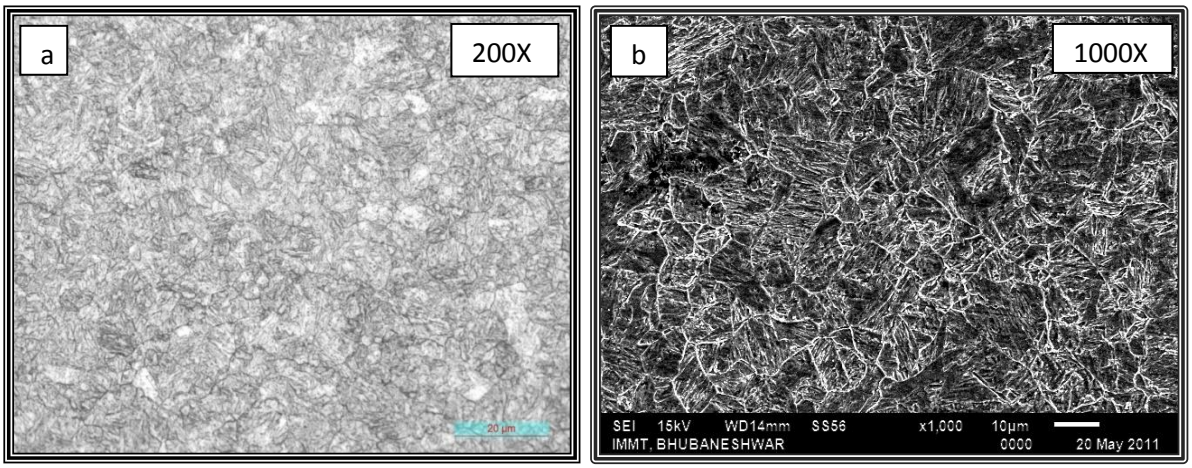

Fig.4.2 (a) Optical micrograph of normalized modified 9Cr-1Mo ferritic steel at 200X (b) SEM micrograph of normalized modified 9Cr -1Mo ferritic steel at 1000X.

4.1.1.1 Phase analysis

Phase analysis of above two composition of ferritic steels can be seen in Fig.4.3. In case of normalized modified 9Cr -1Mo ferritic steel, the % of bainite has high value compared to normalized 2.25Cr-1Mo ferritic steel. It is only due to the higher % of Cr in modified 9Cr -1Mo ferritic steel.

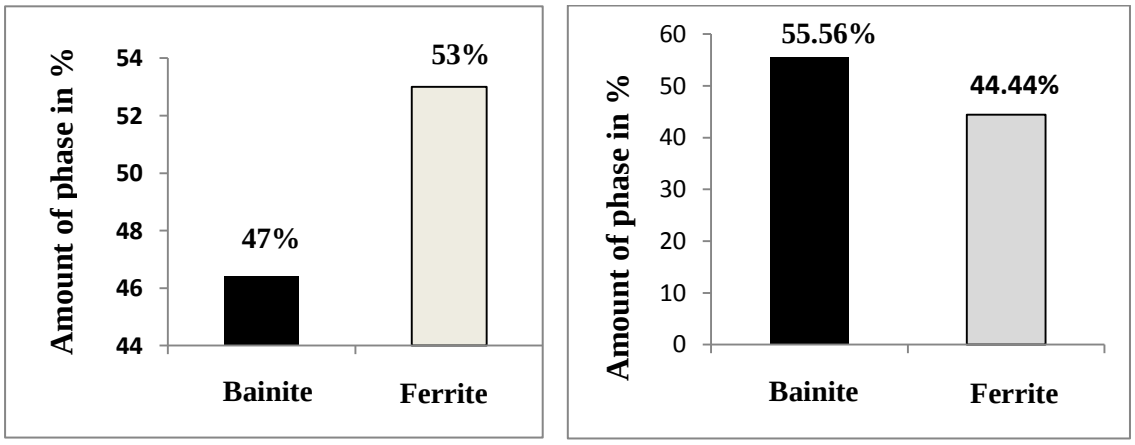

Fig.4. 3 (a) (left) Amount of phases in optical micrograph of normalised 2.25Cr-1Mo steel, (b) (right) Amount of phases in optical micrograph of normalised modified 9Cr-1Mo steel.

4.1.1.2 EDS Analysis

To determine the elements present in normalized 2.25Cr-1Mo and modified 9Cr-1Mo ferritic steels , EDS analysis was done. EDS spectra of investigated samples are shown in Fig.4.4. From that figure it was observed that in both the steels content large amount of Cr and also indicated presence C.

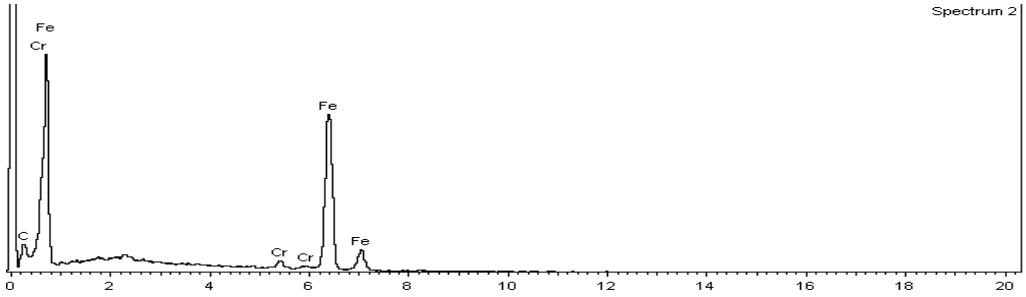

Fig.4.4.(a) EDS Analysis of normalised 2.25Cr-1Mo steel .

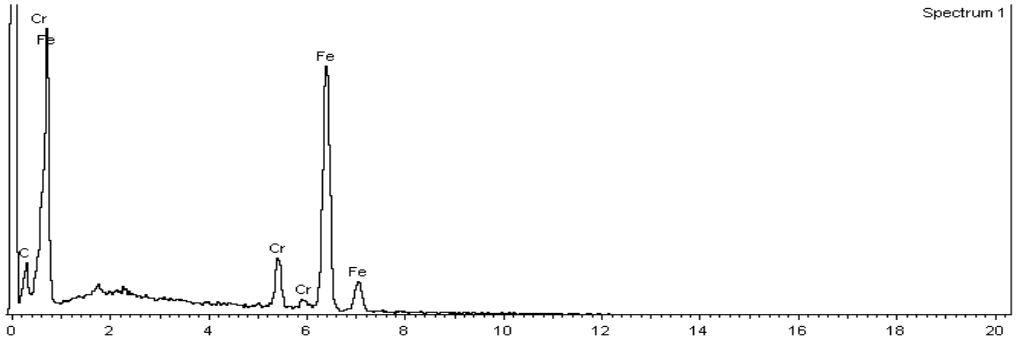

Fig.4.4.(b) EDS Analysis of normalised modified 9Cr-1Mo steel .

4.1.2 Mechanical Properties

4.1.2.1 Hardness

Hardness of investigated samples are shown in Table 4.1. It is observed that the hardness value is more in case of normalized modified 9Cr-1Mo ferritic steel. This is due to high amount of bainite in this heat treated steel.

Table.4.1 Hardness value of normalized 2.25Cr-1Mo and normalized modified 9Cr-1Mo ferritic steels

	Normalised 2.25Cr-1Mo	Normalized modified 9Cr-1Mo steel
HVN	**323**	**398**

4.1.2.2 Tensile Properties

Tensile Properties of investigated samples are shown in Table 4.2. It is observed that the yield strength and tensile strength are more in case of normalized modified 9Cr-1Mo ferritic steel. This is again due to high amount of bainite in this heat treated steel.

Table.4.2 Tensile Properties of normalized 2.25Cr-1Mo and modified 9Cr-1Mo steels

	Yield strength	Tensile strength	% Elongation
Normalised 2.25Cr-1Mo	272.55MPa	496.8MPa	33
Normalized modified 9Cr-1Mo	444.87MPa	601.37MPa	25

4.2. Indentation creep analysis of normalized 2.25Cr-1Mo steel at different temperatures and a load of 10kg

Indentation creep curves of normalized 2.25Cr-1Mo steel at different temperatures (480^0C, 500^0C, 520^0C) and fixed load of 10kg are examined in this section. Indentation creep curve is expressed in the form of depth of indentation Vs time curve. A typical illustration is shown in Fig. 4. 5. The creep rate is calculated according to the standard ASTM 139-07 for each curve. These values are shown in Fig.4.6. The results indicate that creep rate increases with increase in temperature. This may be due to increase rate of diffusion at elevated temperature.

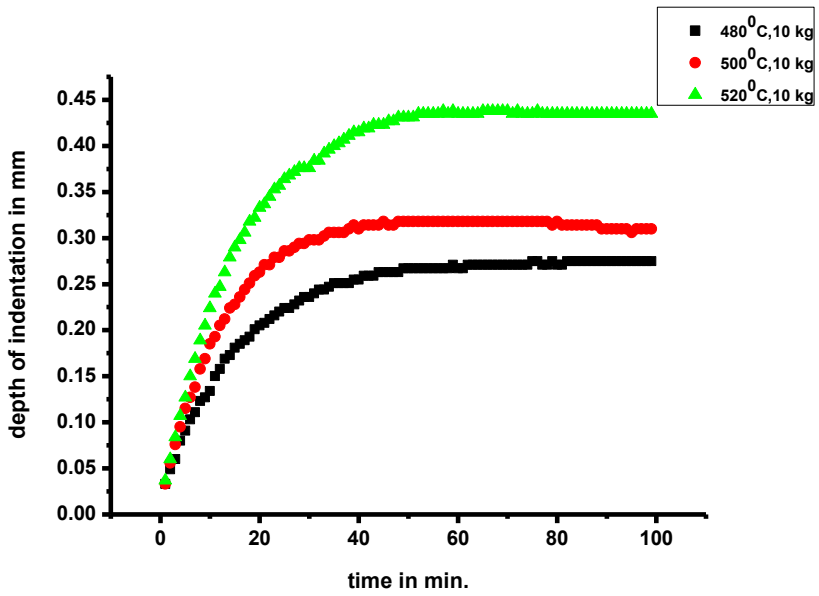

Fig .4.5. Indentation creep curves of normalized 2.25Cr-1Mo steel at different temperature (480^0C, 500^0C, 520^0C) with a constant load of 10kg.

Log (creep rate (mm/min.)) Vs 1/T is plotted in Fig.4.7 to determine the activation energy for creep. The slope of the curve determines the activation energy. Slope is equal to –Q/R.The activation energy was found to be 95kJ/mol. Creep rate Vs time graph is shown in Fig.4.8. Creep rate for all temperature and load has a maximum value at the initial creep stage and it decreased dramatically and finally approached to minimum value after a period of holding time.

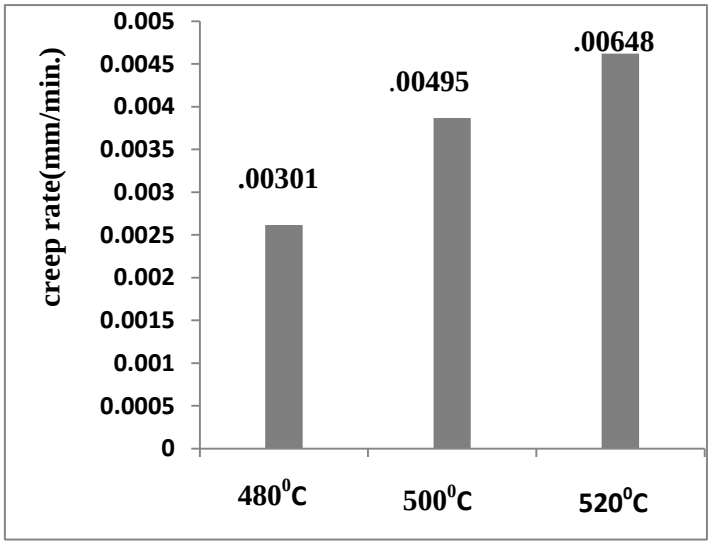

Fig.4.6 Creep rate of normalized 2.25Cr-1Mo steel at different temperatures (480^{0}C, 500^{0}C, 520^{0}C) with a constant load of 10kg.

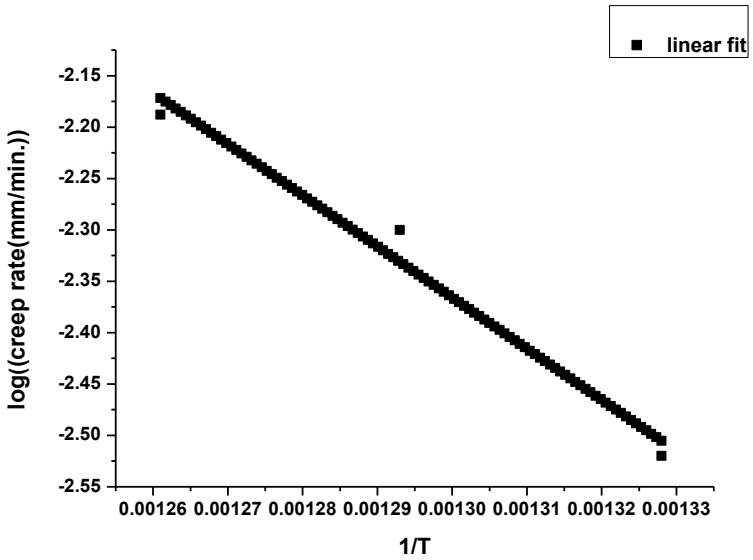

Fig.4.7 Log–log plot of creep rate ἐ vs. 1/T

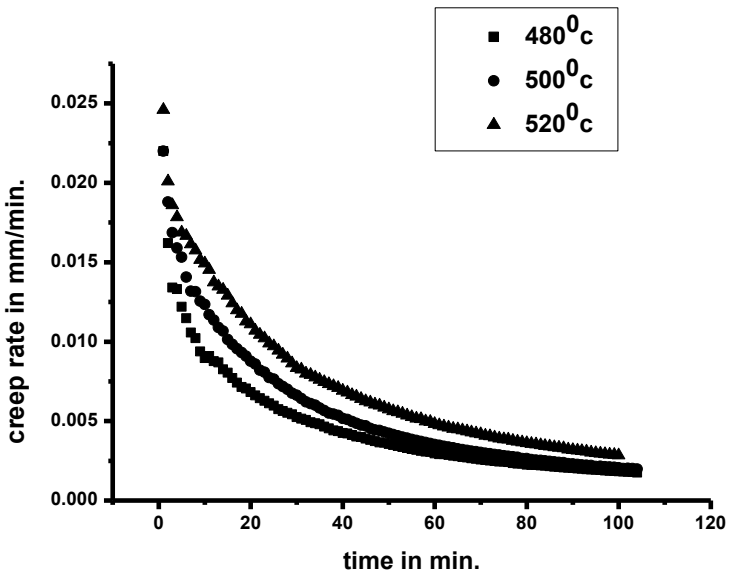

Fig.4.8 Creep rate Vs time graph of normalized 2.25Cr-1Mo steel at different temperature (480^0C, 500^0C, 520^0C) with a constant load of 10kg.

4.2.1 Microstructural analysis

Typical optical and SEM micrographs of post indented creep of normalized 2.25Cr-1Mo steel at 480^0C, 10kg is illustrated in Fig. 4.9. Some ferrite grains are revealed out as compared to the normalized 2.25Cr-1Mo steel. Phase analysis of the microstructure is illustrated in Fig.4.10. It is observed that the amount of bainite is 43.75 % and the amount of ferrite is 56.25%. Typical optical and SEM micrographs of post indented creep of normalized 2.25Cr-1Mo steel at 500^0C; 10kg is illustrated in Fig.4.11. It shows more ferrite grain than the post indented creep of normalized 2.25Cr-1Mo steel at 480^0C with a load of 10kg. Phase analysis of this microstructure is illustrated in Fig.4.12. It contains 37.2% of bainite and 62.8% ferrite and the optical and SEM micrographs of post indented creep of normalized 2.25Cr-1Mo steel at 520^0C, 10kg is shown in Fig. 4.13. The phase analysis of this micrographs (Fig.4.14) shows that the bainite content is 35.9% and the ferrite content is 64.1%. Comparision of amount of different phases before and after indentation creep is shown in Fig.4.15. It is observed that the amount of bainite is gradually decreasing and the ferrite content is increasing. This is because with the increase in indentation creep temperature , the bainite is gradually dissolving. Comparision of hardness value of normalized 2.25Cr-1Mo steel before and after indentation creep is shown in Fig.4.16. It seems to be increase in indentation creep temperature, the hardness is decreasing. The reduction in hardness is attributed to the less amount of bainite and a commensurate change in the distribution of bainite.

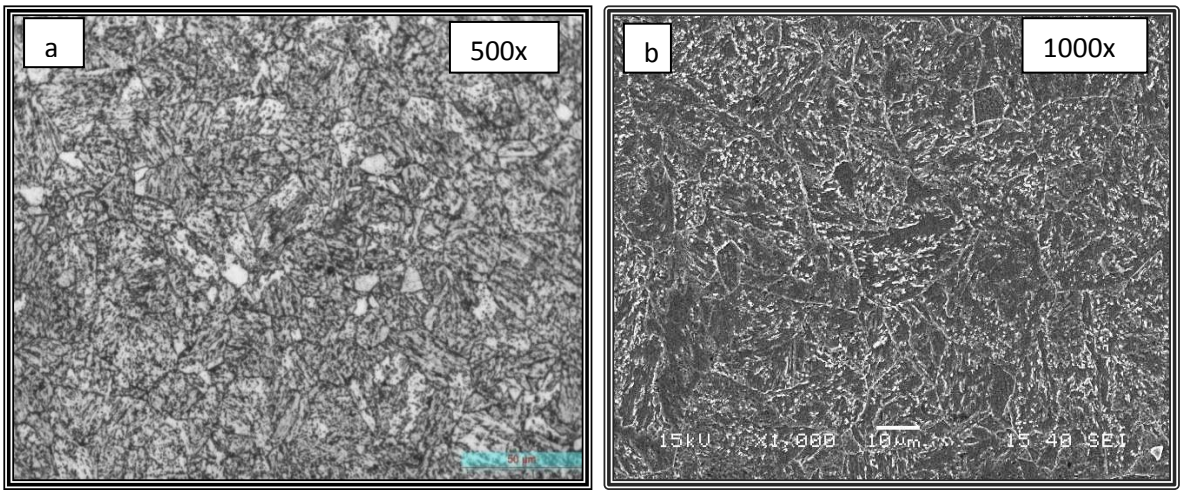

Fig.4.9 Optical micrograph at 500X (b) SEM micrograph of post indented creep of normalized 2.25Cr-1Mo ferritic steel (at 480^0C,10kg)at 1000X.

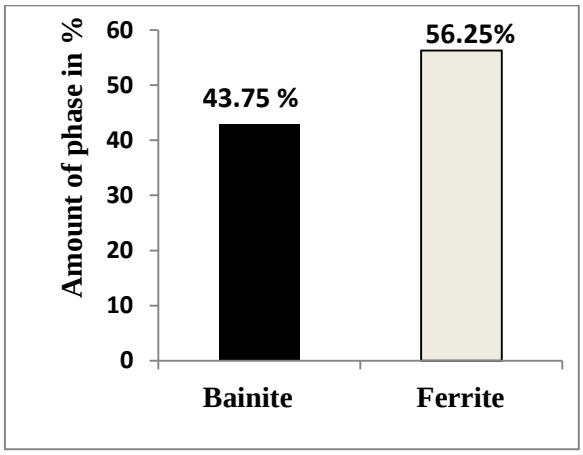

Fig.4.10 (a) Amount of phases in optical micrograph of post indented creep of normalised 2.25Cr-1Mo steel (at 480^0C, 10kg).

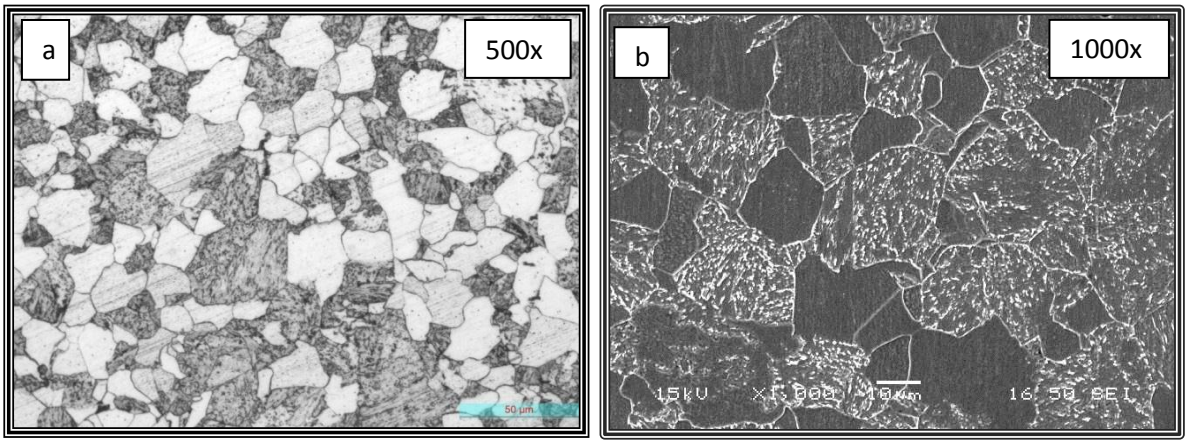

Fig.4.11.Optical micrograph at 500X (b) SEM micrograph of post indented creep of normalized 2.25Cr-1Mo ferritic steel (at 500^0C, 10kg) at 1000X.

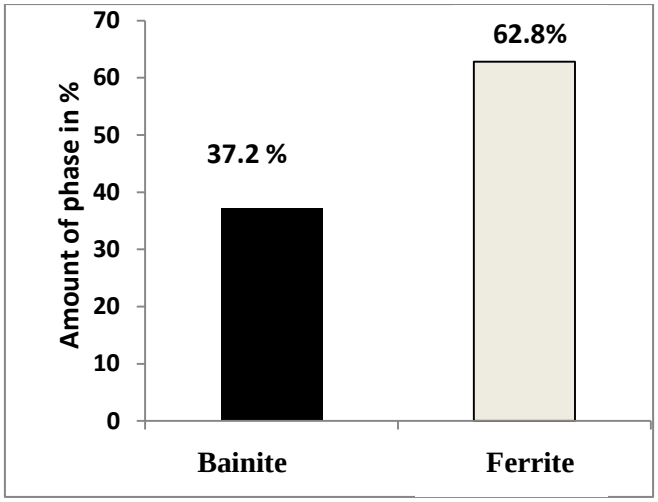

Fig.4.12. (a) Amount of phases in optical micrograph of post indented creep of normalised 2.25Cr-1Mo steel (at 500^0C,10kg).

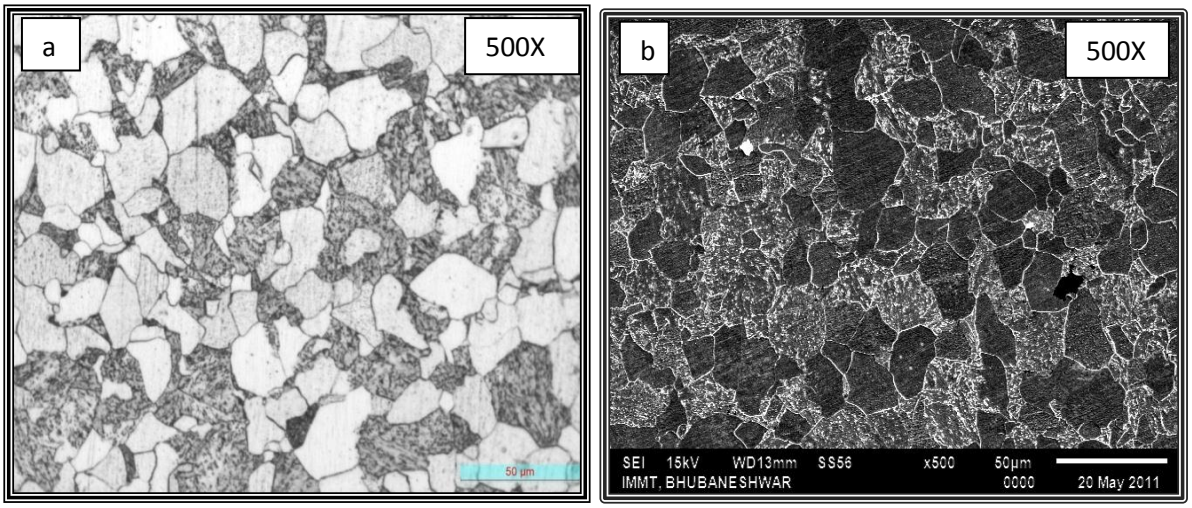

Fig.4.13.Optical micrograph at 500X (b) SEM micrograph of post indented creep of normalized 2.25Cr-1Mo ferritic steel (at 520^0C,10kg)at 500X.

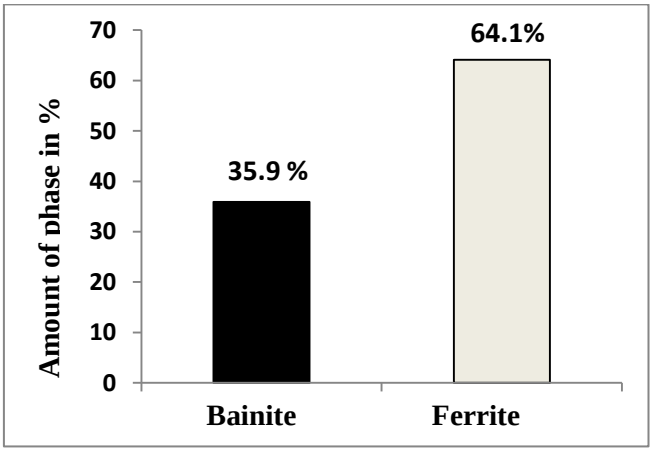

Fig.4.14. (a) Amount of phases in optical micrograph of post indented creep of normalised 2.25Cr-1Mo steel (at 520^0C,10kg) .

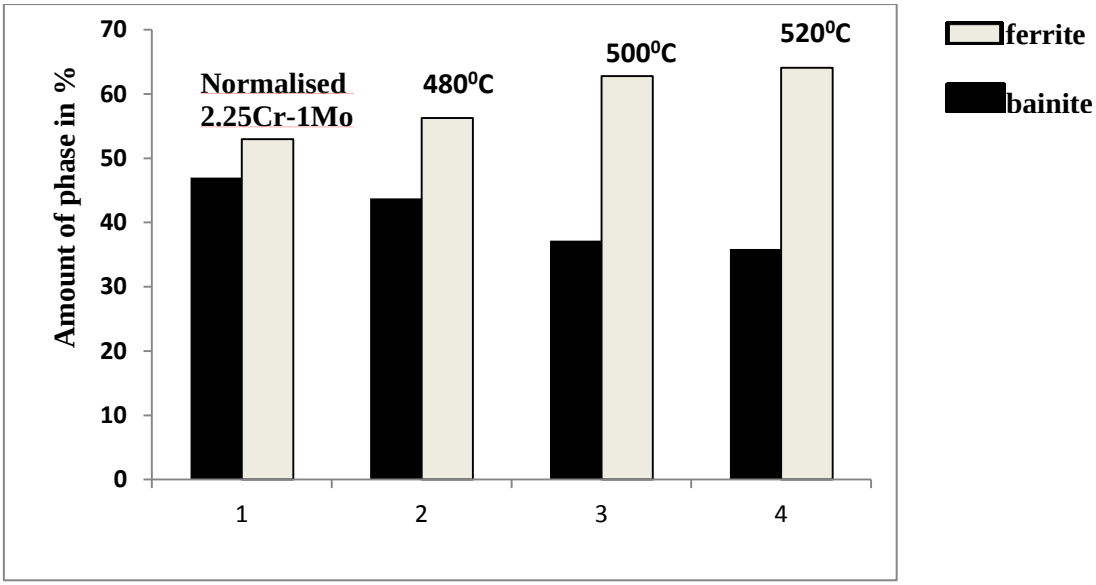

Fig.4.15 Comparision of amount of different phases before and after indentation creep .

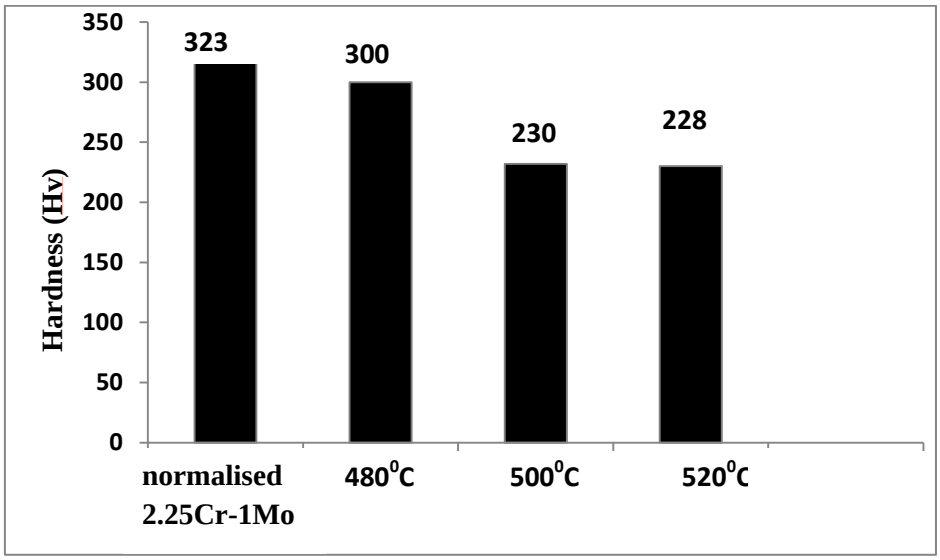

Fig. 4.16 Hardness value of normalized 2.25Cr-1Mo steel before and after indentation creep.

4.3. Indentation creep analysis of normalized 2.25Cr-1Mo steel at 520^{0}C with different load (10kg, 20kg)

Indentation creep curves of normalized 2.25Cr-1Mo steel at 520^{0}C and different load of (10kg.20kg) are examined. A typical illustration is shown in Fig. 4.17. The calculated creep rate is shown in Fig.4.18. The results indicate that creep rate increases with increase in load. Because stress induces the movement of vacancies, dislocation and dislocation jog [21]. The Creep rate Vs time graph of normalized 2.25Cr-1Mo steel at 520^{0}C with different load (10kg, 20kg) also follows the same trend as that of different temperature indented specimen is

shown in Fig.4.19. The optical and SEM micrographs of post indented steel at 520^{0}C and 20kg is examined and illustrated in Fig.4.20. The phase analysis of this microstructure is shown in Fig.4.21. Comparison of amount of different phases of normalized steel at load levels 10kg, 20kg (Fig.4.22) reveals that the amount of bainite is more in case of specimen subjected to 20kg load. This is due to the occurrence of enhanced stress induced transformation. The hardness comparison (Fig.4.23) indicates that the hardness is more in case of 20kg load. This is due to the same reason as mentioned above.

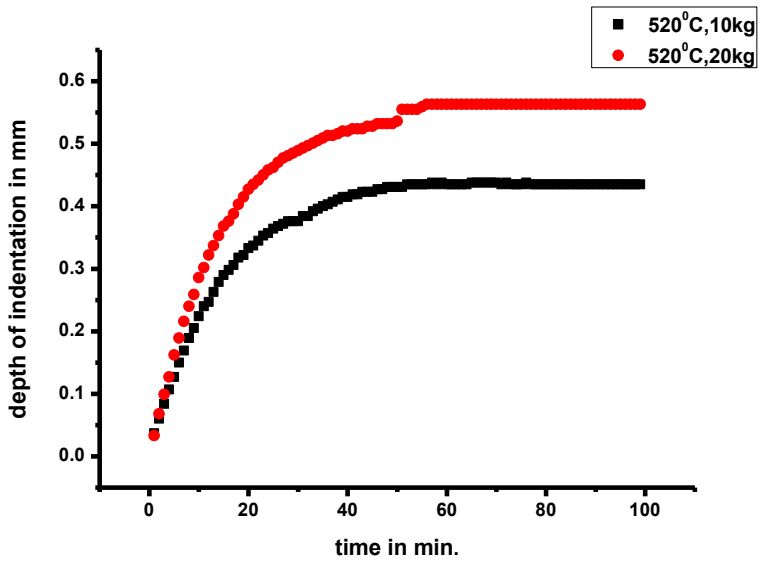

Fig. 4.17 Indentation creep curves of normalized 2.25Cr-1Mo steel at 520^{0}C with different load (10kg, 20kg).

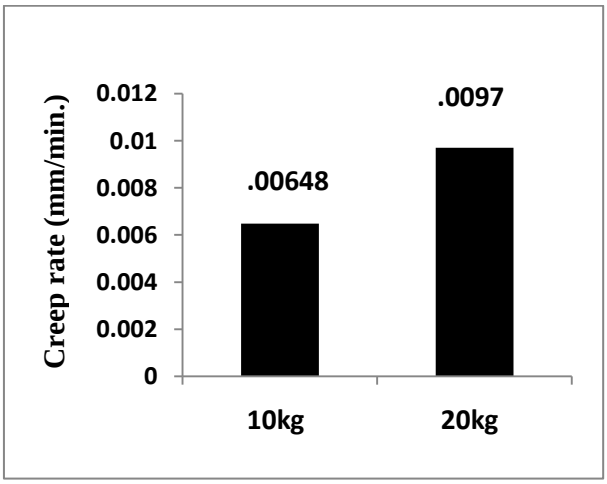

Fig. 4.18 Creep rate of normalized 2.25Cr-1Mo steel at 520^{0}C with different load (10kg, 20kg).

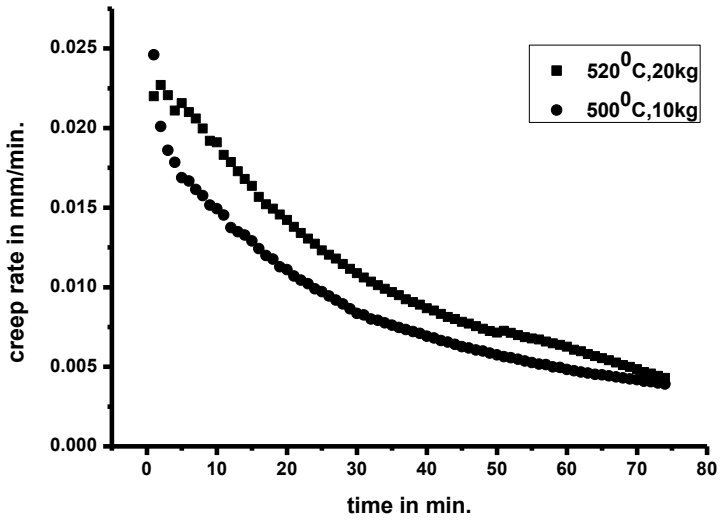

Fig.4.19 Creep rate Vs time graph of normalized 2.25Cr-1Mo steel at 520^{0}C with different load (10kg, 20kg).

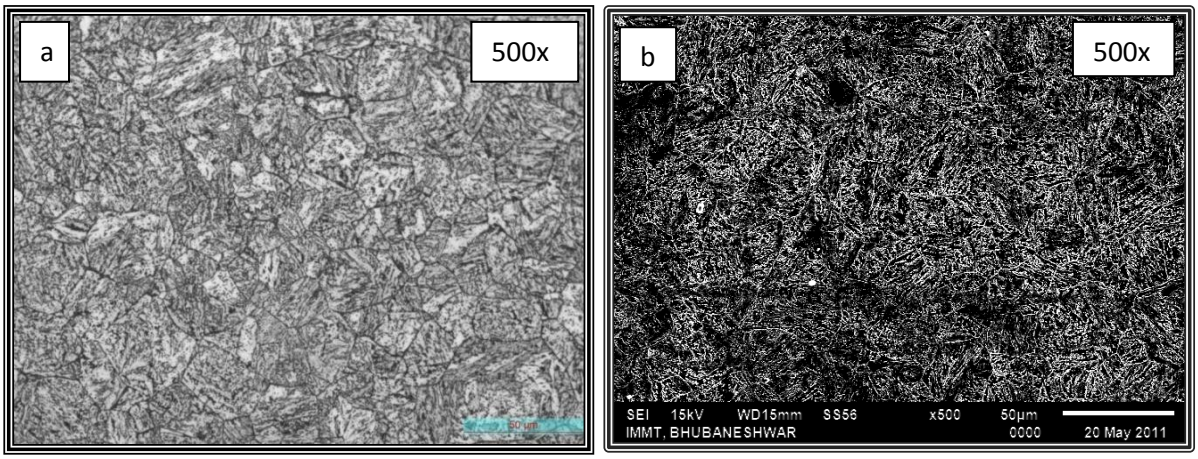

Fig.4.20 Optical micrograph and (b) SEM micrograph of post indented creep of normalized 2.25Cr-1Mo ferritic steel (at 520^{0}C, 20kg) at 500X.

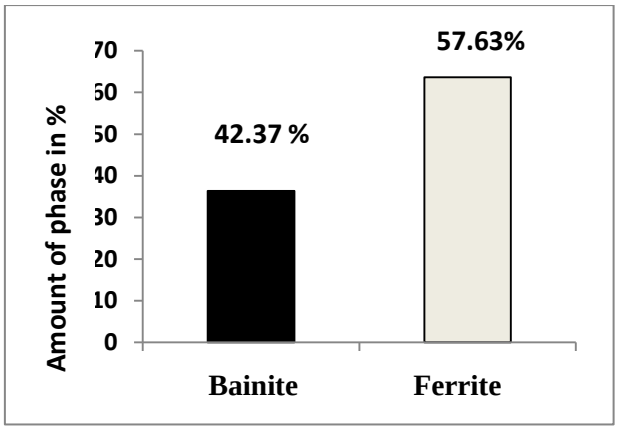

Fig.4.21 (a) Amount of phases in optical micrograph of post indented creep of normalised 2.25Cr-1Mo steel (at 520^{0}C, 20kg) .

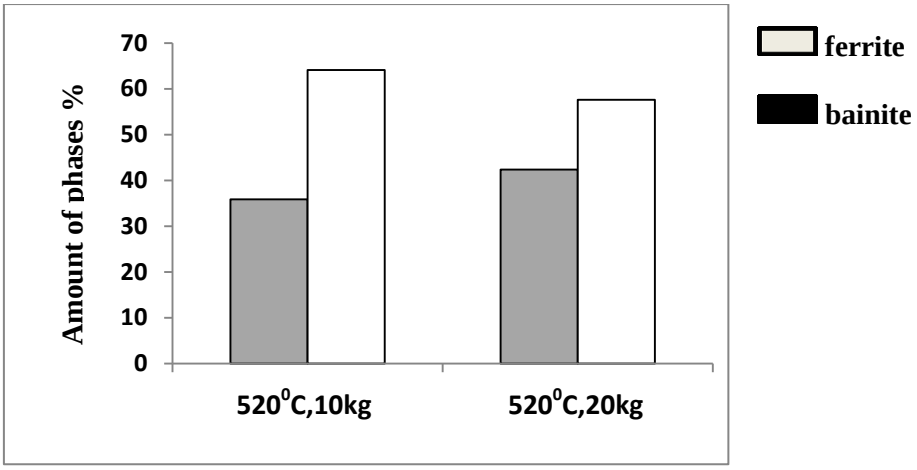

Fig.4.22 Comparision of amount of different phases of normalized 2.25Cr-1Mo steel at 520^0C with different load 10kg,20kg.

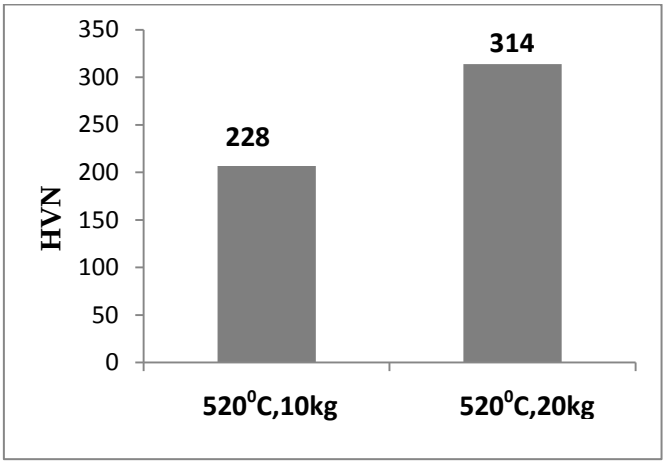

Fig.4.23 Comparision of hardness value of normalized 2.25Cr-1Mo steel at 520^0C with different load (10kg,20kg).

4.3. Indentation creep analysis between normalized 2.25Cr-1Mo steel and normalized modified 9Cr-1Mo steel at 520^0c with a load of 20kg.

The indentation creep curves of 2.25Cr-1Mo and 9Cr-1Mo ferritic steels at 520^0C with a load of 20kg are shown in Fig.4.24. Calculated creep rate is shown in Fig. 4.25. For Creep rate Vs time graph (Fig.4.26), the creep rate is gradually decreasing with the progress of holding time. The optical and SEM micrographs of post indented creep of normalized modified 9Cr-1Mo ferritic steel (at 520^0C, 20kg) is shown in Fig.4.27. The phase analysis shows that bainite content is 40.74% and ferrite content is 59.26%. When comparison of phase analysis (Fig.29) and hardness (Fig.4.30) is done between normalized 2.25Cr-1Mo steel and normalized modified 9Cr-1Mo steel, it is found that the hardness is more in case of

normalized modified 9Cr-1Mo steel. This is due to the high tensile strength and hardness of the steel which is principally due to the presence of larger amount of bainite in the microstructure of 9Cr-1Mo steel. The higher amount of Cr and presence of V may have enhanced that effective dislocation barrier at elevated temperature. This may be a reason of lower creep rate of modified 9Cr-1Mo steel.

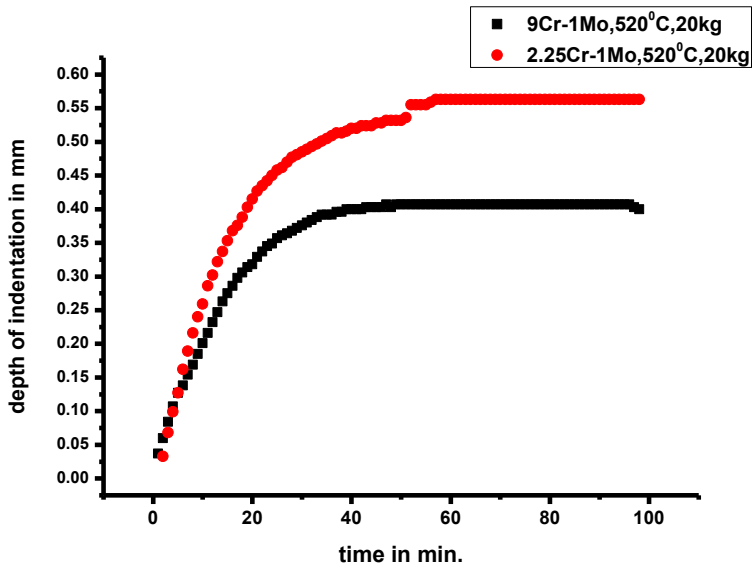

Fig.4.24 Indentation creep curve of normalized 2.25Cr-1Mo and normalized modified 9Cr-1Mo steel at 520^0C with a load of 20kg.

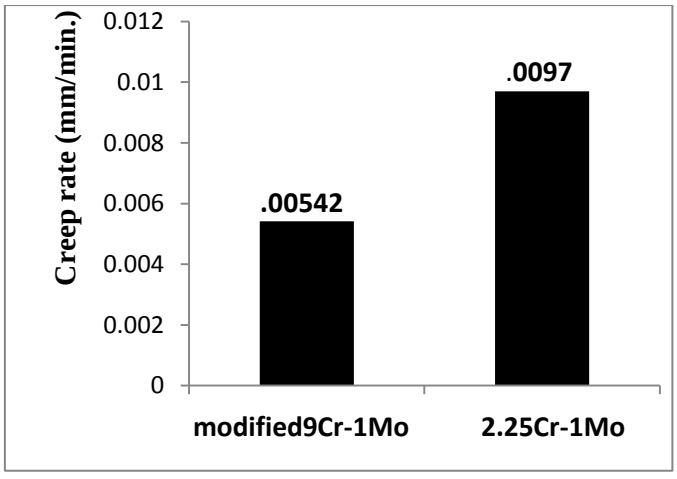

Fig. 4.25 creep rate of normalized 2.25Cr-1Mo and normalized modified 9Cr-1Mo steel at 520^0C with a load of 20kg.

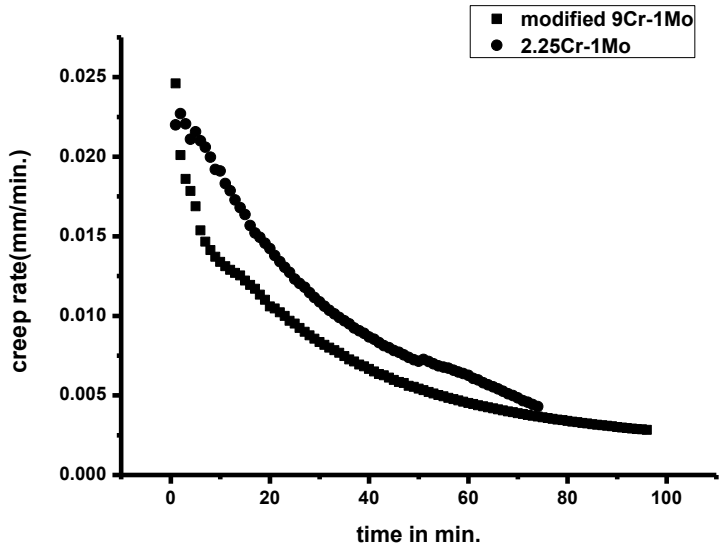

Fig.4.26 Creep rate Vs time graph of normalized 2.25Cr-1Mo steel at 520^0c with different load (10kg, 20kg).

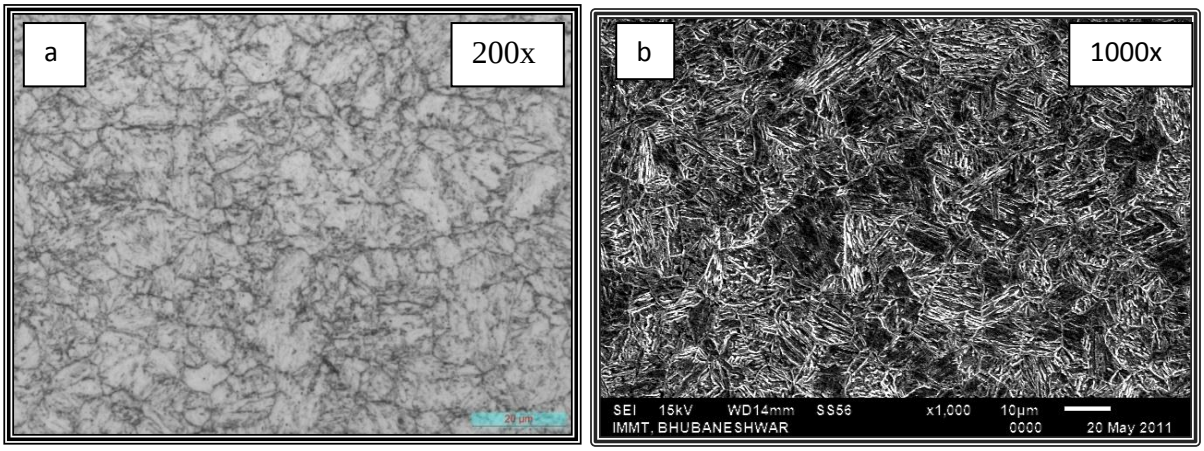

Figure 4.27 Optical micrograph and (b) SEM micrograph of post indented creep of normalized modified 9Cr-1Mo ferritic steel (at 520^0c,20kg)at 500X.

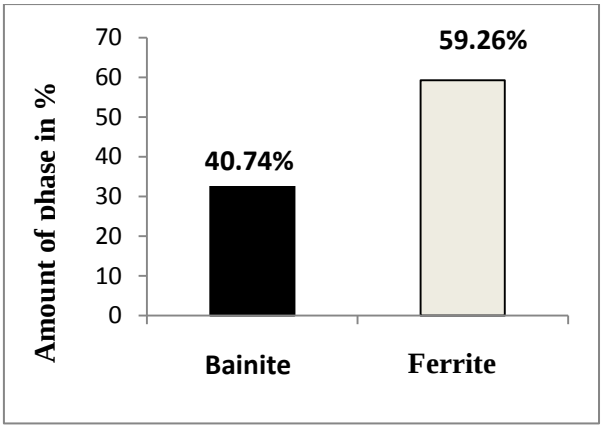

Fig.4.28 Amount of phases in optical micrograph of post indented creep of normalised modified 9Cr-1Mo steel (at 520^0c,20kg) .

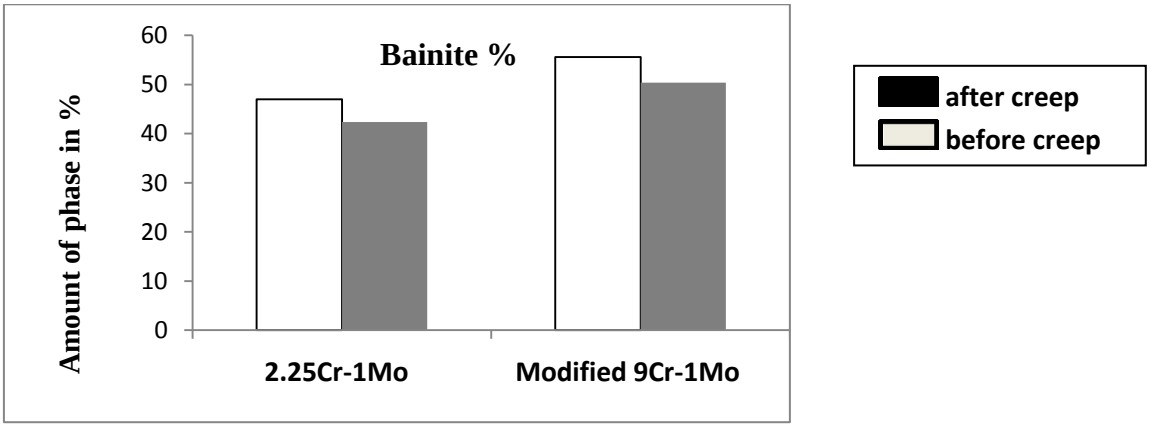

Fig.4.29 Comparision of amount of phases before and after creep of normalized 2.25Cr-1Mo steel and normalized modified 9Cr-1Mo steel at 520^0c with a load of 20kg.

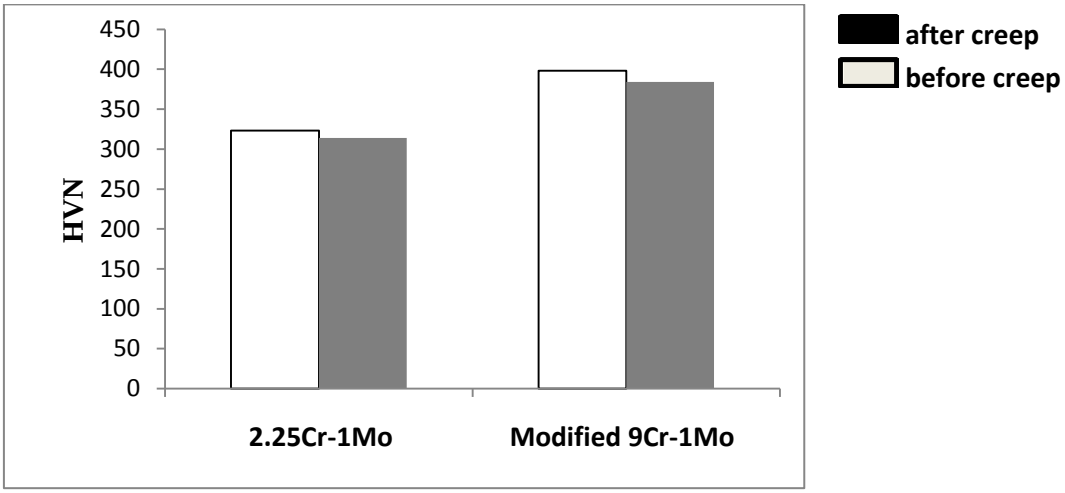

Fig.4.30 Comparision of hardnes value of normalized 2.25Cr-1Mo steel and normalized modified 9Cr-1Mo steel at 520^0C with a load of 20kg before and after creep.

CHAPTER 5

Conclusions

Chapter 5

5. Conclusions

- ✓ Creep of 2.25Cr-1Mo ferritic steel was load and temperature dependent, larger load and higher temperature resulted in a larger creep deformation.
- ✓ Creep rate for all temperature and load had a maximum value at the initial creep stage and it decreased dramatically and finally approached to minimum value after a period of holding time.
- ✓ The value of activation energy (Q) for creep was found to be 95 kJ/mol.
- ✓ It was observed that with increase in temperature there is a decline in creep strength because there is a reduction in the amount of bainite with the progress of temperature.
- ✓ The modified 9Cr-1Mo ferritic steel alloy shows the best compressive creep behaviour because of higher amount of alloying element.

Scope for future work

- ✓ Experimentation may be done using large number of sample for better accuracy and refinement of the proposed materials.
- ✓ The complex failure mechanism of creep in 2.25Cr-1Mo and 9Cr-1Mo steel requires TEM analysis for a better characterization of these materials.
- ✓ Evaluation can be done on Indentation creep behaviour after 520^0C temperature and loading capacity up to 30 kg.

References

1. Ray et al A.K., Materials Science and Engineering A, 454–455 (2007):pp. 679–684.

2. Islam M.A., ARPN Journal of Engineering and Applied Sciences .1 (2006): pp. 1819-6608.

3. Arivazhagan B., Prabhu Ranganath, Albert S.K., Kamaraj M., and Sundaresan S., Journal of Materials Engineering and Performance, 18(8) (2009): pp.1000.

4. Dobrzanski J., Zielinski A., Krzton H., Journal of Achievements in Materials and Manufacturing Engineering, 23(2007).

5. Fujita T., Advanced Materials and Processes, 141 (1992): pp. 42-47.

6. Hald J., International journal of Pressure Vessels and Piping, 85 (2008): pp. 30-37.

7. Yoshizawa M. and Igarashi M., International journal of Pressure Vessels and Piping, 84 (200): pp. 30-37.

8. Klueh R.L., International Materials Reviews, 50 (2005): pp. 287-310.

9. Scheu C.,Kauffmann F., Zies G., Maile K., Straub S., Mayer K.H., Zeitschrift Fur Metallkundne, 96 (2005): pp. 653-659.

10. Buschow K.H.J., Elsevier, Amsterdam, Netherland (2001).

11. Diehl H. and Granacher J., Archifor Das Eisenhettenwesen, 50 (1979): pp. 299-303.

12. Dubey J.S., Chilukuru H., Chakravartty J.K., Schwienheer M., Scholz A., Blum W., Metallurgical and Materials transactions A, 406 (2005): pp. 152-159.

13. Kadoya Y., Goto T., Date S., Yamauchi T., Saida T., ISIJ International, 30 (1990): pp. 854-861.

14. Kimura A., Kasada R., Kohyama A., Tanigawa H., Hirose T., Shiba K., Jitukawa S., Ohtsuka S., Ukai S., Sokolov M., Klueh R.L., Yamamoto T. and Odette G.R., Journal of Nuclear materials, 367 (2007): pp. 60-67.

15. Knezevic V., Balun J., Sauthoff G., Inden G. and Schneider A., Metallurgical and Materials transactions A, 477 (2008): pp. 334-343.

16. Gandy G., X20CrMov12-1 steel handbook, Electrical power research institute palo alto, USA (2006).

17. Vicente Braz Trindadea, Rodrigo Borinb, Behzad Zandi Hanjari , Materials Research,8 (2005): pp. 365-369.

18. Sundararajan T., Kuroda S., Kawakita J., Seal S. Surface & Coatings Technology 201 (2006): pp.2124–2130.

19. Shankar Vani, Valsan M. , Kannan R., Bhanu K. Rao Sankara, Mannan S.L.and Pathak S.D., International Symposium of Research Students on Materials Science and Engineering (2004).

20. Jha B.B., Mishra B.K., Sahoo T.K., Mukherjee P.S. and Ojha S.N,Defect and Diffusion Forum, 303-304 (2010): pp. 85-97.

21. G E.Dieter, Mechanical Metallurgy. UK, McGraw Hill (1988).

22. Naumenko K. and Altenbach H., Springer-Verlag (2007).

23. Graham A, Walles K. , JISI (1955): pp.105.

24. Phillips F. , Philos Mag (1905): pp.513.

25. McVetty P G. , Trans ASME (1933); pp.55-99.

26. Conway JB, Mullikin MJ.Proceedings of AIME conference, Detroit, Michegan (1962).

27. Norton FN. , New York: McGraw-Hill (1929).

28. Nadai A., Stephen Timoshenko anniversary volume. New York: Macmillan (1938).

29. McHenry D., Proc ASTM, 43(1943): pp.1069.

30. Kachanov L., Izv Akad Navk. SSR, 8(1958): pp.26.

31. Rabotnov Y. Amsterdam: North-Holland (1969).

32. Sandstrom R., Kondyr A., third international conference on mechanical behavior of materials, Cambridge (1979).

33. Westbrook. J., Trans Am Soc Met, 45 (1953): pp.221.

34. Atkins A., Met Sci, 16 (1982):pp.127.

35. Underwood E., Mater Meth, 45 (1957): pp.127.

36. Geach G., Int Met Rev, 19 (1974): pp.255.

37. Li W, Warren R., Acta Metall Mater, 41 (1993): pp.3065.

38. Heynes M. S. R., Rawson H., Phys. Chem. Glass. 2/1 (1961): pp.1.

39. Douglas R. W., Armstrong W. L., Edward J. P. and Hall D., Glass Tech. 6/2 (1965): pp.52.

40. Yu E. C., and Li J. C. M., Phil. Mag. 36 (1977): pp.911.

41. Yu E.C. and Li J. C. M., Mater. Sci. 12 (1977): pp. 2200.

42. Chu S. N. G., Li J. C. M., J.Mater. Sci. Eng., 39 (1979): pp. 1

43. Chu S. N. G., Li J. C. M. J.Appl. Phys., 51 (1980): pp. 3338.

44. Yu H. Y., Imam M. A., Rats B. B., J. Mat. Sci., 20 (1985): pp. 636.

45. Tasnadi P., Juhasz A., Chinh N.Q., Kovacs I. Res. Mech., 24 (1988): pp. 334.

46. Juhasz A., Tasnadi P., Szaszvari P., Kovacs I., J. Mat. Sci., 21 (1986): pp. 3287.

47. Chinh N.Q., Juhasz A., Tasnadi P., Lendvai J., Kovacs I., phys. Stat. Sol. (a), 138 (1993): pp. 175.

48. Chinh N.Q., Juhasz A., Tasnadi P., Kovacs I., Kovács-Csetenyi E., J. Mat. Sci. 29 (1994): pp. 2341.

49. Chinh N.Q., Illy J., Juhasz A., Lendvai J. phys. stat. sol. (a), 149 (1995): pp. 583.

50. Sneddon I. N., Int. J. Eng. Sci., 347 (1965): pp. 245.

51. Tasnadi P., Juhasz A., Chinh N.Q, Szaszvari P.and Kovacs I. Mater. Sci. Forum, 13/14 (1987): pp. 421.

52. Hyde T.H, Yehia K.A, Becker A.A, Int. J. Mech. Sci., 35, N6 (1993): pp. 451.

53.Kutty T.R.G., Kumar A.,Kamath H.S., Trans. IIM 63(2010): pp. 443-447.

CONFERENCE

[1] **National conference:**B.B.Verma, Manila Mallik, P.K Ray, "*Fatigue crack initiation and growth behavior of 7475 Aluminum alloy in air and aggressive envioronments"*22nd Annual General meeting materials research society of India, Feb 14-16-2011.

[2] **National conference:**B.B.Verma, Manila Mallik, P.K Ray, "*Mechanisum of corrosion fatigue in structural alloys "*22nd Annual General meeting materials research society of India, Feb 14-16-2011.